Adsorption study of toxic metal ions using functionalized 3D mesostructured silica

Nagy Torad
Tanta University

Ahmed Abu El-Nasr
Tanta University

Nehal Salahuddin
Tanta University

mohamad ayad (✉ mohamad.ayad@ejust.edu.eg)
E-JUST: Egypt-Japan University of Science and Technology   https://orcid.org/0000-0002-6678-1773

Research Article

Adsorption study of toxic metal ions using functionalized 3D mesostructured silica

Nagy L. Torad,[a] Ahmed Abu El-Nasr,[a] Nehal A. Salahuddin,[a] Mohamad M. Ayad[*a,b]

[a] Department of Chemistry, Faculty of Science, Tanta University, Tanta 31527, Egypt

[b] School of Basic and Applied Sciences, Egypt-Japan University of Science and Technology (E-JUST), New Borg El-Arab City, Alexandria 21934, Egypt

*Corresponding Email: Mohamad.ayad@ejust.edu.eg

Abstract

Mesoporous silica KIT-6 was chemically modified using 3-mercaptopropyltriethoxysilane (3-MPTS) *via* post-grafting method to prepare functionalized mesoporous KIT-6-SO$_3$H with highly acidic –SO$_3$H groups. Thin layers of KIT-6-SO$_3$H coating onto quartz crystal microbalance (QCM) electrodes are employed as a meso-KIT-6-QCM sensor for the adsorptive removal of Pd(II), Cd(II) and Cs(I) ions with a high detection sensitivity. From ICP-OES measurements, the calculated adsorption capacity (Q_e) values are much coincide with that obtained from QCM sensor. Due to the synergetic cooperation between high surface area, large pore volumes and active –SO$_3$H groups, KIT-6-SO$_3$H exhibited a remarkable adsorption capacity for metal ions. The effect of initial solution pH on the metal ions uptake was carefully studied. Kinetics and isotherm studies further reveal that adsorption of metal ions by KIT-6-SO$_3$H obeys second-order kinetic and Langmuir isotherm, respectively.

Keywords: Mesoporous silica KIT-6; post-grafting; quartz crystal microbalance (QCM); nanosensor; ICP-OES measurements

1. Introduction

Pollution is the main concern that damage human life and ecosystems. In the past few years, efforts have been done by scientists to decrease the effect of environmental pollution [1]. In particular, toxic heavy metals are carcinogenic represent a major pollutant of waste streams [2], because they are tended to accumulate in living organisms without biodegradation [3,4]. For example, radioactive ^{137}Cs contaminates with high mobility are dissolved in soils and finally transported in plants, then animals and consequently become a part of human beings [5]. The so-released radionuclide ^{137}Cs fallout from nuclear power plant to the environment damages the ecosystem owing to its relatively long half-life time (30.2 years), high activity (emits gamma radiation) and volatility. As it exists in a monovalent state, Cs(I) is high soluble and quickly migrates in aquatic environments and tends to remain in an available form to biota for several decades [6]. In addition, toxic Pb(II) replaces calcium and then accumulate in the skeletal system [7]. Water-containing large Pb(II) content causes various neuro effects, hypertension, cardiovascular diseases, reduced renal function, as well as decreased fertility, and adverse pregnancy results [8,9]. Further, Cd(II) is also toxicant for animals and results in abnormalities and affects the liver, kidney, nervous and immune systems [10,11]. The Environmental Protection Agency (EPA) included Cd(II) on the "red list" of significance substances because longtime exposure to human body causes lung cancer and kidney disease including proteinuria, however, short-term affects the lung through inhalation [12]. Therefore, treatment of industrial effluents with high toxic metals content before being released into the environment is urgently needed for protecting the environment and human health.

So far, for the past few decades, various methods have been utilized for heavy metal ions remediation, such as chemical precipitation [13], colorimetry [14], membrane filtration [15], electrochemical sensors [16,17], precipitate flotation [18], biological treatments [19], coagulation [20], ion exchange [21,22] and adsorption [23,24]. Among the available technologies, adsorption is recognized as one of the most effective methods for its simplicity, low cost, availability of materials and generally

yield high-quality treated effluents [25]. In this regard, the overall performance of an adsorptive separation technique is directly dependent on the effectiveness of the adsorbent material; various noble adsorbents, such as zeolites [26], activated carbon [27,28], functionalized polymers [29,30], clay minerals [31], chitosan [32] and cellulose materials [33] have been reported so far. However, some of these adsorbents are either inadequate due to diffusion limitation or insufficient surface functionalities which decrease their detection sensitivity.

Recently, advances in the nanostructured materials to develop advanced detection systems have been reported by several research groups [34–36]. A special attention has been paid to mesoporous silica materials for their cost effectiveness and high-performance toward removal of toxic metals in wastewater treatment systems [37,38]. Despite their considerable advantages over others in sensing materials, there is still a growing demand increase the adsorption capability for environmentally important toxic species with a rapid-assessment process. Synthesis of mesoporous silica with a large mesostructured properties and active functionality could remarkably enhances the adsorptive removal of toxic ions. In this context, for further increase the adsorption capability, chemical modification of pore walls surface of mesoporous silica by organic functional groups *via* either *co*-condensation or *post*-grafting methods were applied [39–45]. Although, several studies investigated the utilization of organic active groups functionalized mesoporous silica materials as promising adsorbents [46–52], a few reports have been demonstrated for the use of functionalized KIT-6 [53–59].

In this paper, we present the synthesis of sulphonated mesoporous silica, KIT-6-SO$_3$H *via* post-grafting method with a high -SO$_3$H groups content. We successfully designed a quartz crystal microbalance (QCM) sensor modified with high surface area KIT-6-SO$_3$H (meso-KIT-6-QCM) for the detection of toxic metals ions with high adsorption affinity. The sensor binds efficiently with Pb(II) than that in case of Cd(II) and Cs(I) ions. The large difference in binding constant (K_a) values is very crucial for sensor selectivity. From QCM and UV-Vis spectroscopy studies, KIT-6-SO$_3$H showed impressive

adsorption capacities for Pb(II), Cd(II) and Cs(I). In addition, for comparison, inductively coupled plasma combined with optical emission spectrometry (ICP-OES) measurements were conducted for quantifying these trace elements at low levels. The sensitivity, adsorption capacity and reusability were investigated. The adsorption kinetic and isotherm models were carefully discussed, as well.

2. Experimental

2.1 Chemicals

Triblock poly(ethylene oxide)-*b*-poly(propyleneoxide)-*b*-poly(ethyleneoxide) copolymer Pluronic® P123 (Mw 5800), tetraethylorthosilicate (TEOS, 98%) and sodium polystyrene sulfonate (PSS), polydiallyldimethylammonium chloride (PDDA) were purchased from Sigma-Aldrich. 3-Mercaptopropyltriethoxysilane (3-MPTS) from MP biomedicals. *n*-Butanol, ethanol and toluene were purchased from HPLC Fisher. Hydrochloric acid (35%), sulphoric acid (36%) and hydrogen peroxide were purchased from ADWIC, Egypt. Standard solutions of Pb, Cd and Cs ions (1000 mg·L^{-1}) were purchased from CPAChem (C.P.A Ltd, Bulgaria). Cs standard solution (1000 mg·L^{-1}) was purchased from Wako Pure Chemical Industries, Ltd, Japan. All raw chemicals were used without any further purification.

2.2 Synthesis and functionalization of mesoporous silica KIT-6

Mesoporous silica KIT-6 was synthesized based on the sol-gel method reported previously [60]. Typically, 12 g of hydrochloric acid (35%) was added to a solution of Pluronic® P123 (6.0 g) dissolved in 220 mL distilled water. The clear homogeneous solution was added to 6 g of *n*-butanol and stirred at 35 °C for 1 h. Then, a 12.48 g TEOS was added to the mixture dropwise, with a continuous stirring for 24 h at room temperature. After that, the solution mixture was refluxed at 100 °C for 24 h. The final product was then filtered, washed with distilled water thrice and dried at room temperature and then calcined in air at 550 °C to obtain mesoporous silica KIT-6.

The functionalization of mesoporous silica KIT-6 with sulphonate groups was conducted by simple post-grafting method with propyl thiol groups followed by a chemical oxidation to obtain $-SO_3H$ groups [60]. In a typical procedure, 3.0 g of KIT-6 was immersed in dry toluene (25.0 g) and refluxed under N_2 gas atmosphere for 1 h. Then, 3-MPTS was added dropwise, and the mixture continued refluxing for 48 h. The obtained thiol-functionalized KIT-6 (KIT-6-SH) was kept for few hours and then was filtered, washed with toluene and ethanol thrice, and dried in a convection oven at 80 ^{o}C for 24 h. After that, KIT-6-SH was converted into sulphonate-functionalized KIT-6 (denoted as KIT-6-SO$_3$H) *via* chemical oxidation of KIT-6-SH (2.0 g) using an excess amount of H_2O_2 (30 wt.%, 20 mL) for 12 h under N_2 gas atmosphere. Finally, KIT-6-SO$_3^{-2}$ was readily protonated with acidified H_2SO_4 (0.05 M) for 2 h. The resultant KIT-6-SO$_3$H material was then filtered, washed with distilled water thrice and dried in a convection oven at 80 ^{o}C for 24 h.

2.3 Adsorption study using QCM measurements

The adsorptive removal of metal ions by KIT-6-SO$_3$H was carefully studied using QCM technique (meso-KIT-6-QCM). Before drop-coating, QCM electrodes were firstly cleaned with ethanol and dried at 50 ^{o}C. Then, their fundmental frequencies (F_0) were recorded. A suspension solution of KIT-6-SO$_3$H (1.0 mg·mL^{-1}) was prepared in an aqueous solution of Nafion® and sonicated for 30 min. Thin films of KIT-6-SO$_3$H were deposited by drop-coating method onto Au-quartz electrodes, then were kept at room temperature for 30 min. After that the electrodes coated with KIT-6-SO$_3$H were placed in drying overnight in an oven at 50 ^{o}C. The electrode coated with KIT-6-SO$_3$H was then fixed inside the QCM instrument and the frequency after coating was measured as F_1 and then used for estimating the mass amount of KIT-6-SO$_3$H coated QCM electrode based on Eq. 2.

The meso-KIT-6-QCM electrode was immersed in 140-mL working cell containing distilled water and the time-dependent frequency was recorded until reached equilibrium. After that, a standard metal ions solution (1.0 mL of 1000 mg·L^{-1}) were successively injected into the working cell. The

response was very fast, and the frequency was immediately decreased due to the fast adsorption uptake of metal ions into the mesoporous KIT-6-SO₃H films. The frequency of QCM sensor was automatically recorded on a PC-supported programming system. All measurements were carried out under the same conditions in air-conditioned atmosphere.

The resonant frequency of the crystal was measured using a Fluke/Phillips PM 6654 frequency counter. By measuring the decrease in frequency, the mass per unit area (m, g·cm^{-2}) of KIT-6-SO₃H deposited onto the QCM electrode was estimated. The maximum adsorption capacity of KIT-6-SO₃H film for metal ions and the apparent association constant (K_a) of the metal ions binding were derived from Langmuir equilibrium binding isotherms were estimated by the following equation [61]:

$$\Delta F = \frac{[M^{n+}]\Delta F_{max}}{K_d+[M^{n+}]} \tag{1}$$

where K_d (M) is the equilibrium dissociation constant and it is equal reverse of the equilibrium association constant, $1/K_a$ (M^{-1}). The relationship of ΔF to the mass change (Δm, g·cm^{-2}) of the adsorbed metal ions into the KIT-6-SO₃H is defined by the Sauerbrey equation [62].

$$\Delta F = -\left(\frac{2F_0^2}{\sqrt{\rho_Q\mu_Q}}\right)\Delta m \tag{2}$$

where F_o (Hz) is the fundamental resonance frequency of the quartz crystal, ρ_Q is the quartz density (2.649 g·cm^{-3}), and μ_Q is the shear modulus (2.947 x 10^{11} g·cm^{-1}·s^{-2}). To estimate the sample amount, ΔF of the KIT-6-SO₃H film was obtained as 1165 Hz, thus the sample amount coating on the Au-electrode of QCM was estimated to be 40 μg·cm^{-2}.

Desorption of metal ions was conducted by immersing the metal-containing KIT-6-SO₃H in distilled water, followed by addition of diluted HNO₃ (0.01 M, 100 mL) at room temperature. The maximum desorption amount of Pb(II), Cd(II) and Cs(I) from the KIT-6-SO₃H film coated QCM electrodes were estimated from the following equation.

$$\%Removal = 100(C_0 - C_e)/C_0 \tag{3}$$

2.5 UV-Vis absorption spectroscopy measurements

A stock solutions (100 mg·L^{-1}) of Pb(II), Cd(II) and Cs(I) (standard metal nitrate solutions, 1000 mg·L^{-1}) were prepared in distilled H$_2$O. KIT-6-SO$_3$H powder (4.0 mg) was immersed in 50 mL of metal ion solution (100 mg·L^{-1}) and the mixture was then stirred at 700 rpm at different time intervals. Then, the solution was quickly centrifuged at 7000 rpm and the supernatant was withdrawn by a syringe into the quartz-cuvette. The initial and final concentration of each metal ion were determined by UV-Vis absorption spectroscopy. The ICP-OES measurements were conducted to quantify the trace elements at low levels after adsorption.

The maximum adsorption capacity of metal ions was investigated by mixing metal ions solutions of various concentrations with mesoporous KIT-6-SO$_3$H (4.0 mg) for 8 h until an equilibrium has been attained. The amounts of metal ion adsorbed into a unit weight of KIT-6-SO$_3$H, Q_e (mg·g^{-1}), is calculated from the mass balance equation.

$$Q_e = (C_0 - C_e).V.m^{-1} \qquad (4)$$

To investigate the adsorption kinetics of Pb(II), Cd(II) and Cs(I) over KIT-6-SO$_3$H, the pseudo-first order, pseudo-second-order and intraparticle-diffusion were applied to fit the experimental data [63]. The pseudo-first-order rate expression expressed as follows:

Pseudo- first order: $\log(Q_e - Q_t) = \log Q_e - \dfrac{k_1}{2.303}t$ \qquad (5)

The pseudo-second-order rate reaction is also expressed as following:

Pseudo-second order: $t/Q_t = 1/k_2 Q_e^{\ 2} + t/Q_e$ \qquad (6)

Intraparticle diffusion: $Q_t = k_i t^{1/2} + C$ \qquad (7)

where Q_e (mg·g^{-1}) is the amount of adsorbed metal ions at equilibrium and Q_t (mg·g^{-1}) is the amount of adsorbed metal ions at time t (min). k_1 (min^{-1}) is the adsorption rate constants of pseudo-first order, k_2

$(g \cdot mg^{-1} \cdot min^{-1})$ is the adsorption rate constants of pseudo-second order and k_i $(mg \cdot g^{-1} \cdot min^{-1})$ is the intraparticle diffusion rate parameter.

The equilibrium adsorption data were investigated using Langmuir, Freundlich and Tempkin models according to the following equations [64]:

Langmuir isotherm: $\qquad C_e / Q_e = 1/K_l + a_l C_e / K_l$ $\qquad\qquad$ (8)

Freundlich isotherm: $\qquad \ln Q_e = \ln K_f + 1/n \ln C_e$ $\qquad\qquad$ (9)

Temkin isotherm: $\qquad Q_e = B \ln K_t + B \ln C_e$ $\qquad\qquad$ (10)

where C_e is the equilibrium concentration of the adsorbate $(mg \cdot L^{-1})$, Q_e is the amount of adsorbed per unit mass of adsorbent $(mg \cdot g^{-1})$, K_l $(L \cdot mg^{-1})$ is a constant related to the affinity between the adsorbent and the adsorbate, K_l/a_l is the theoretical monolayer saturation capacity Q_o, n is Freundlich constants and $K_f [(L \cdot mg^{-1})1/n]$ is constant correlated to the maximum adsorption capacity, K_t is the equilibrium binding constant and corresponds to the maximum binding energy and B is constant related to the heat of adsorption.

2.5 Instruments and materials characterization

The morphological structure of the functionalized mesoporous silica KIT-6-SO$_3$H was checked by the transmission electron microscope (TEM, S4800 X2.0 KV 8.1mm X120K TE). N$_2$ adsorption-desorption isotherms were obtained by Nova 3200e Quantachrome Autosorb automated system at 77 K. The UV-Vis absorption spectra were collected using UV-Vis spectrophotometer (UVD-2960 Labomed, Inc). Quantitative metal ions analysis was performed with inductively coupled plasma-optical emission spectrometers (ICP-OES) (Agilent Technologies, ICP-700 series, Australia) equipped with a concentric nebulizer and a cyclonic spray chamber. An absorption standard solution of the corresponding metal (100 ppmv in water) was used to calibrate the equipment. The FT-IR Spectrometer (Bruker, Tensor 27 model) is used to measure IR spectra. Thermogravimetric (TG) analysis was conducted in air by using Perkin Elmer STA from 25 to 800 °C with a heating rate of 5 °C·min^{-1}. Low-angle X-Ray powder diffraction

patterns were measured using GNR, APD 2000 PRP step scan X-ray diffractometer using monochromated Cu Kα radiation (40 kV, 40 mA) at a scanning-rate of $1^o \cdot min^{-1}$. Small-angle X-ray scattering (TI-SAXS) measurements were conducted using a NANO VIEWER (Rigaku, Japan) equipped with a Micro Max-007 HF high-intensity micro-focus rotating anode X-ray generator by using monochromated Cu Kα radiation (λ= 0.1540 nm).

3. Results and discussion

3.1 Structure characterization

Chemical modification of mesoporous silica KIT-6 with active –SO₃H groups that covalently attached to silanol groups (Si-OH) was successfully realized. From TEM observations (Figure 1A), a 3D interconnected cubic mesoporous KIT-6 with a pore diameter of *ca.* 12.2 nm is formed. After functionalization to obtain KIT-6-SO₃H, TEM clearly shows that the cubic well-ordered mesostructure of KIT-6 is still retained, however the pore size is slightly decreased to 8.2 nm, as a result of successful sulfonation of KIT-6 with PrSO₃H groups *via* post-grafting method (Figure 1B). From SAXS, KIT-6 exhibits three identical well-resolved diffraction peaks centered at 2θ= 1.015°, 1.219° and 1.500° which can be indexed as (211), (220) and (321) planes of a 3D cubic mesostructured pristine KIT-6 ($Ia\bar{3}d$) with a d_{211} spacing of 9.04 nm, respectively, as shown in Figure 1C(a) [60]. In contrast to pristine KIT-6, functionalized KIT-6-SO₃H shows broadened and less-resolved diffraction peaks at 2θ= 1.016°, 1.213° and 1.494°, assignable to (211), (220) and (321) planes, respectively, indicating the successful functionalization of the silica inner pore wall surfaces with PrSO₃H groups. The same phenomenon is also observed from the low-angle XRD measurements (Figure 1D). As clearly observed, pristine KIT-6 shows a well-resolved diffraction peak at 2θ= 0.9, indexed as (211) plane (Figure 1D(a)), indicating the formation of a highly ordered structural with a *bcc* space group symmetry of $Ia\bar{3}d$, similar to those previously reported for KIT-6 materials [60]. By contrast, low-angle XRD of the functionalized KIT-6-SO₃H reflects the broadening of (211) plane as shown in Figure 1D(b).

9

Figure 1. (A&B) TEM images of pristin mesoporous silica KIT-6 and functionalized KIT-6-SO₃H, respectively. TEM image of the original KIT-6 and KIT-6-SO₃H (($Ia\bar{3}d$) space group) taken with the incident beam parallel to the [111] direction. (C&D) small-angle SAXS measurements and low-angle XRD patterns of (a) KIT-6 and (b) KIT-6-SO₃H, respectively.

Functionalization of KIT-6 with PrSO₃H groups was carefully investigated by the FT-IR measurements, as well (Figure S1, in the supporting information). FT-IR spectrum of the pristine mesoporous silica KIT-6 (Figure S1) displays a number of characteristic bands. The band present at 3435 cm^{-1} and 1630 cm^{-1} are assignable to the stretching vibration of hydrogen bonded silanol groups $\upsilon(\equiv$Si-OH) and O-H bending vibration mode of physisorbed water molecules, respectively. Two characteristic bands of asymmetric and symmetric stretching vibration of Si–O–Si are observed at 1084 cm^{-1} and 820 cm^{-1}, respectively. Upon functionalization, the presence of PrSO₃H is confirmed by the formation of two bands located at 2930 cm^{-1} and 710 cm^{-1} which are characteristic of C–H stretching vibration and C–SO₃H stretching vibration of PrSO₃H, respectively (Figure S1) [60].

The thermal stability of mesoporous silica KIT-6 and KIT-6-SO$_3$H was examined by TG analysis (Figure S2). All samples show an initial weight loss at about 150 °C due to physically adsorbed water molecules. No significant weight loss was observed during the disintegration of pristine KIT-6, implying the high thermally stability of mesoporous silica KIT-6 (Figure S2). After functionalization with PrSO$_3$H, TGA exhibits a broad exothermic peak observed between 300 and 500 °C, which is attributed to the decomposition of organic moieties of PrSO$_3$H groups functionalized mesoporous silica KIT-6 as shown in Figure S2. Compared to pristine KIT-6, KIT-6-SO$_3$H shows a weight loss of *ca.* 31% close to 650 °C, indicating the successful functionalization of KIT-6 with a high content of sulphonate groups.

To explore the mesoporosity, N$_2$ adsorption-desorption isotherms of pristine KIT-6 and KIT-6-SO$_3$H samples were recorded at 77 K (Figure 2). The BET surface areas, mesopore sizes and total pore volumes are summarized in Table 1. All samples displayed type IV isotherms and the adsorbed volume in the adsorption isotherm gradually increases in the range of P/P_0= 0.3–0.8, which is typically associated with the capillary condensation of nitrogen gas in mesopores. In addition, the presence of large hysteresis loops of both pristine KIT-6 and KIT-6-SO$_3$H samples indicating the formation of uniform pore textures with large channel-like mesopores.

Compared to pristine KIT-6, a noticeable decrease of the BET surface area and total pore volume from 1085 m$^2 \cdot$g^{-1} and 0.942 cm$^3 \cdot$g^{-1} for pristine KIT-6 to 860 m$^2 \cdot$g^{-1} and 0.743 cm$^3 \cdot$g^{-1} in case of KIT-6-SO$_3$H was observed (Table 1). Nevertheless, functionalized KIT-6-SO$_3$H still possess high BET surface area. Moreover, the mesopore sizes were slightly decreased from 12.9 nm to 8.8 nm for pristine KIT-6 and KIT-6-SO$_3$H), respectively, which is much coincide with those observed from TEM measurements. These results clearly demonstrate the successful functionalization of KIT-6 with PrSO$_3$H groups into outer and inner pore wall surfaces, retaining the mesostructure ordering of mesopore channels.
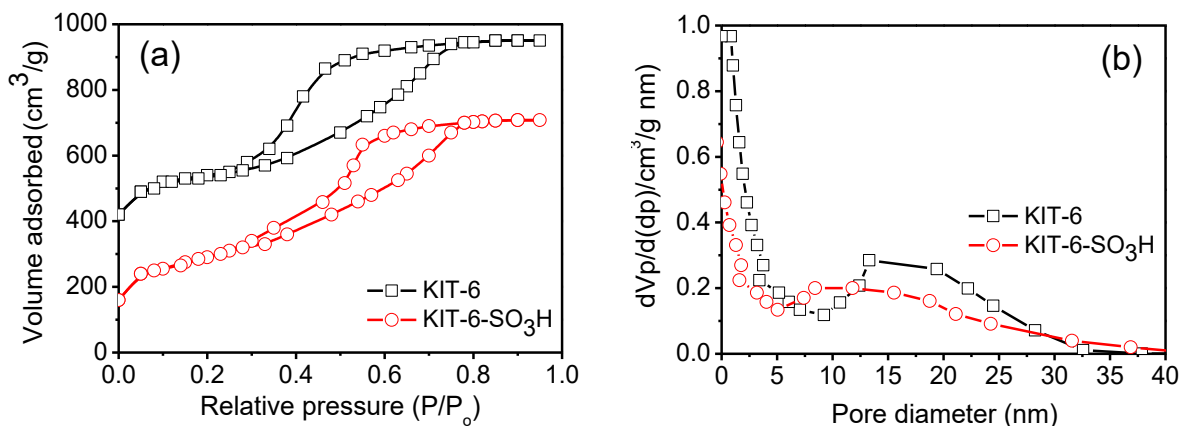
Figure 2. (a & b) Nitrogen adsorption-desorption isotherms and pore size distributions of pristin mesoporous silica KIT-6 (black line) and functionalized mesoporous KIT-6-SO₃H (red line).

Table 1. Textural properties of mesoporous silica KIT-6 materials and functionalized KIT-6-SO₃H.

Samples	Surface area $(m^2 \cdot g^{-1})$	Pore volume $(cm^3 \cdot g^{-1})$	Pore diameter (nm)
KIT-6	1085	0.942	12.9
KIT-6-SO₃H	860	0.743	8.8

3.2 Study of metal ions adsorption behavior

Inspired by the high surface area and active –SO₃H groups, we investigated the utilization of mesoporous KIT-6-SO₃H as an adsorbent material for treating polluted water from toxic metal ions. Here, we design a QCM sensor coated with a thin layer of mesoporous KIT-6-SO₃H for adsorptive removal of Pb(II), Cd(II) and Cs(I) ions. The adsorption behavior of metal ions of interest was also studied by using UV-Vis spectroscopy technique. A QCM is a very sensitive device for precisely sensing mass changes based on changes in the oscillation frequency. Coating of QCM electrodes with various porous materials has been considered as pioneering research for enhancing sensor performance [65−67]. High chemical stability and high BET surface area, as well as presence of active function groups are very crucial for designing QCM sensor. Very recently, we have demonstrated the use of QCM electrodes integrated with –NH₂ and

–SO$_3$H functionalized KIT-6 and SBA-15 with high BET surface areas for pH-responsive drugs loading/release studies [68].

For this purpose, we designed a meso-KIT-6-QCM sensors for the detection of Pb(II), Cd(II) and Cs(I) ions of 10 mg·L^{-1} in water. Time-dependent frequency shift (ΔF, Hz) was recorded as shown in Figure 3. When metals ion solution was injected into the QCM cell, the frequency underwent a dramatic decrease, then reached a steady state within 30 min, implying a high adsorption affinity of mesoporous KIT-6-SO$_3$H toward metal ions. As clearly seen, Pb(II) ions exhibits a higher (ΔF) of 195 Hz, compared with Cd(II) ions (171 Hz) and Cs(I) ions (132 Hz). In addition to the high BET surface area and 3D cubic mesostructure of KIT-6-SO$_3$H, the difference in adsorption affinity towards Pb(II) over Cd(II) and Cs(I) could be attributed to the difference in their ionic size and charge of the cation. It is noted that, the affinity of –SO$_3$H groups functionalized KIT-6 towards metal ions increases with increasing the charge of metal ion. As –SO$_3$H group is a strong acid, a high binding interaction occurs with divalent metal ions, while monovalent Cs(I) exhibit a weak interaction, because of its low charge density or by means of Pearson's Principle [69].

The desorption of Pb(II), Cd(II) and Cs(I) ions from mesoporous KIT-6-SO$_3$H was conducted in distilled water as shown in Figure 3. The removal of Pb(II), Cd(II) and Cs(I) from KIT-6-SO$_3$H reaches 85.6 %, 87.5 % and 91.0 %, respectively. On addition of diluted HNO$_3$ (0.01 M) into water gives rise to desorption amount of metal ion (99.90 %) within 1 h. This good reversibility test is helpful for practical use.
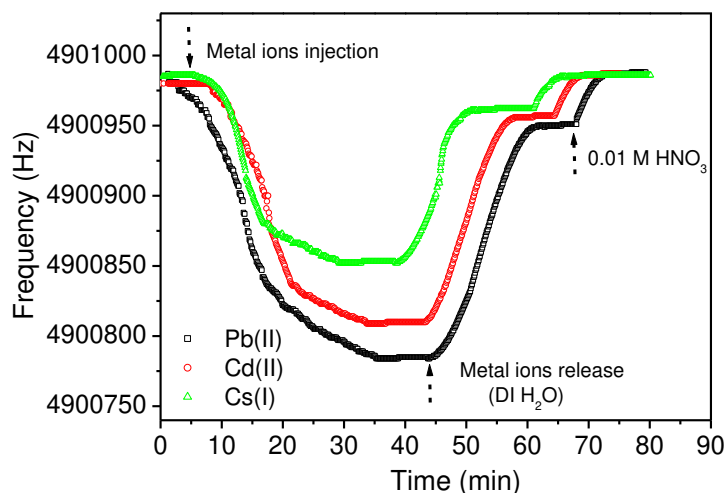
Figure 3. Mass-normalized time-dependence frequency shifts of QCM electrodes coated with KIT-6-SO₃H upon exposure to Pb(II), Cd(II) and Cs(I) ions solutions (after the injection of metals ions solutions (10 ppmv, 10 mL). Release test of Pb(II), Cd(II) and Cs(I) ions was conducted by addition of DI H_2O into the QCM electrode followed by addition of 0.01 M HNO_3.

Furthermore, the maximum adsorption uptake (Δm_{max}) of mesoporous KIT-6-SO₃H film coated QCM sensor for Pb(II), Cd(II) and Cs(I) was carefully investigated. At a given concentration, the plot of maximum adsorption uptake *versus* [Metal ion] showed saturation curves as shown in Figure 4(a). Based on Langmuir binding model (Eq. 1), Figure 4(b) shows linear plots of [Metal ion]/ΔF against [Metal ion], where [Metal ion] indicates the initial concentration of Pb(II), Cd(II) and Cs(I) ions. The corresponding association constants (K_a) and maximum binding uptake (Δm_{max}) of KIT-6-SO₃H for Pb(II), Cd(II) and Cs(I) were calculated from slopes of the linear regressions and intercepts (Figure 4(b)). From Eq. (1), the K_a values for Pb(II), Cd(II) and Cs(I) are calculated as 4.18 M⁻¹, 1.44 M⁻¹ and 1.03 M⁻¹, respectively, implying that Pb(II) ions binds efficiently into mesoporous KIT-6-SO₃H than that in case of Cd(II) and Cs(I) ions. Binding of mesoporous KIT-6-SO₃H with Pb(II) is almost three order of magnitude stronger than Cd(II) and approximately four times larger than Cs(I). The large difference in K_a values is very crucial for sensor selectivity. Additionally, the maximum uptake (Δm_{max}) of KIT-6-SO₃H film coated

QCM electrodes for Pb(II), Cd(II) and Cs(I) ions are estimated as 176 mg·g^{-1}, 154 mg·g^{-1} and 118 mg·g^{-1}, respectively.
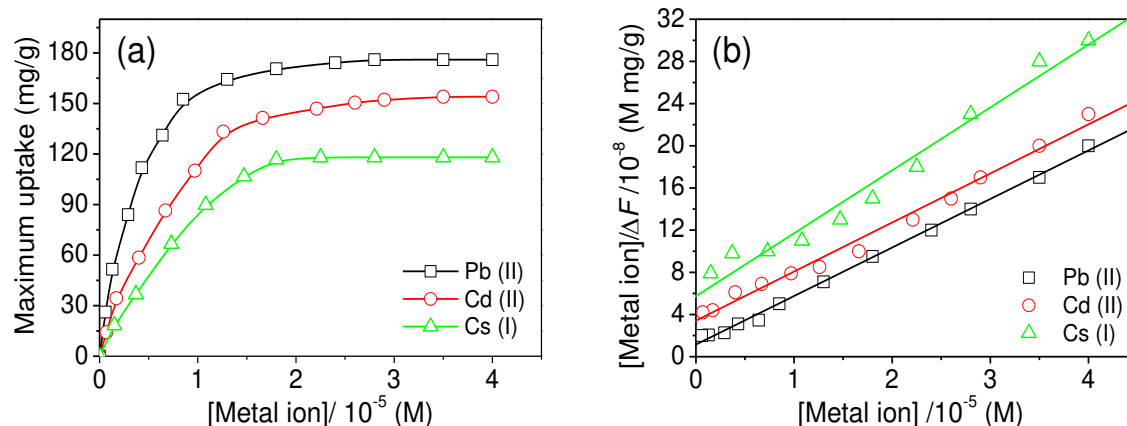

Figure 4. (a) Saturation binding behaviors of Pb(II), Cd(II) and Cs(I) ions depending on concentrations of metal ions at 25 °C. (b) Their linear reciprocal plots of [Metal ion]/ΔF against [Metal ion].

Along with QCM sensor measurements, the adsorptive removal of Pb(II), Cd(II) and Cs(I) over KIT-6-SO$_3$H was carefully studied by UV-Vis absorption spectroscopy. The supernatant was then withdrawn by syringe into a quartz cuvette and the metal ion concentration was measured by UV-Vis spectrophotometer at different time intervals (Figure S3). The concentration of metal ions is sharply decreased with the time. As clearly seen, the adsorption of metal ions into KIT-6-SO$_3$H is rapid at the early stage of contact time, and then approaches equilibrium after a few hours, indicating a fast adsorption uptake of metal ions towards mesopores at the early stage of adsorption process. The synergic cooperation between high BET surface area and large pore diameter induced by the 3D cubic mesostructured of KIT-6 facilitate a high diffusion uptake of metal ions inside the mesopores, as well as active acidic –SO$_3$H groups available for metal complexation. After 6 hours, mesoporous KIT-6-SO$_3$H shows a remarkable adsorption capacity for Pb(II) ions of 123.5 mg·g^{-1}, which is overwhelmingly higher than that of Cd(II) ions (117.5 mg·g^{-1}), and Cs(I) ions (90.6 mg·g^{-1}) as shown in Figure 5. These data coincide with those obtained by ICP-OES analysis (138 mg·g^{-1} for Pb(II) ions, 127.3 mg·g^{-1} for Cd(II)

ions, and 88.1 mg·g^{-1} for Cs(I) ions) and were almost in a good agreement with the data estimated from the QCM sensor technique. The divalent metal cations, Pb(II) with large charge densities strongly complexed with the acidic –SO$_3$H groups leading to remarkably high adsorption affinity. Furthermore, mesoporous KIT-6-SO$_3$H exhibited higher adsorptive removal of *ca.* 99.2 % for Pb(II) ions higher than that in case of Cd(II) ions (92.4 %) and Cs(I) ions (83 %) (Figure 5(b), which is most likely attributed to the difference in their ionic size and charge of the cation (Figure S4).
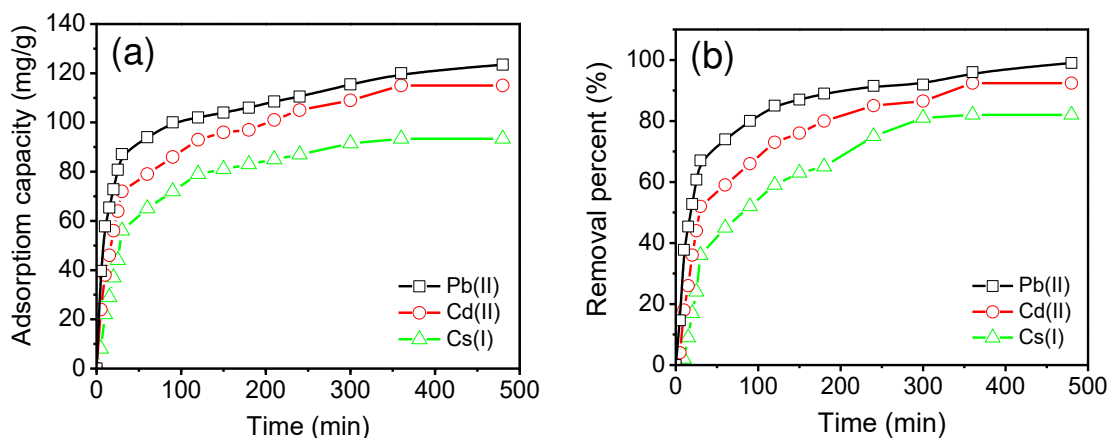

Figure 5. (a) Time-dependent adsorption capacities and (b) removal efficacy of KIT-6-SO$_3$H toward Pb(II), Cd(II) and Cs(I) ions (100 ppmv).

3.2.1 Effect of pH

The effect of pH on the removal efficiency of Pb(II), Cd(II) and Cs(I) ions by KIT-6-SO$_3$H was carefully investigated. Figure 6 shows that the adsorption of metal ions increases with increasing the solution pH from 3.0 to 5.5 (the metals ions precipitating as metal hydroxides at pH ≥ 6.0). In this pH ranges, the removal efficiency of KIT-6-SO$_3$H for metal ions dramatically decreases when the solution pH is decreased as the positive surface charge enhances the repulsive forces between metal ions and –SO$_3$H groups, thus reducing the adsorption capacity. In highly acidic solution (decreasing pH), the competition between the present H$^+$ and metals ions probably decreases the complexing affinity between metal ions and –SO$_3$H groups functionalized KIT-6-SO$_3$H because it tends to be protonated. The acidic –SO$_3$H

16

functional groups act as efficient active sites for complexing metal ions, probably based on the following

suggested mechanism [70,71]:

$$-SO_3H + M^{+n}_{(aq)} \rightleftharpoons -SO_3M + H^+_{(aq)}$$
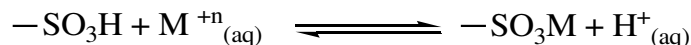
By decreasing the H^+ concentration (increasing pH), the equilibrium shifts to the right-hand side, thus

the adsorption affinity for the metal ions increases as shown in Figure 6.
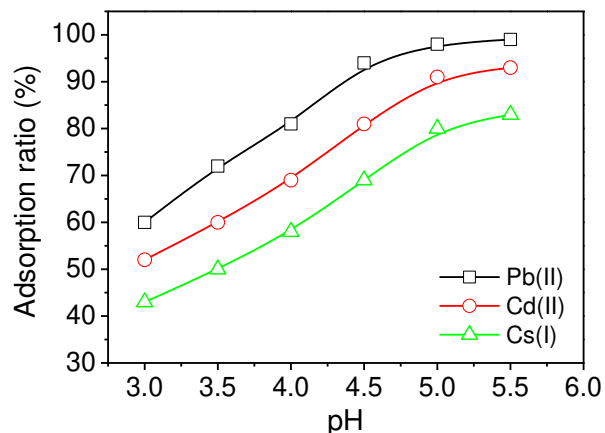

Figure 6. The effect of pH on the removal percentage of Pb(II), Cd(II) and Cs(I) ions by functionalized
mesoporous silica KIT-6-SO₃H.

3.2.2 Adsorption kinetics

In order to evaluate the adsorption mechanism that controls the kinetics of adsorption of Pb(II), Cd(II)

and Cs(I) ions into KIT-6-SO₃H. At metal ions uptake, the experimental data was analyzed using

different kinetic models, such as pseudo-first order, pseudo-second-order and intraparticle diffusion

models [63]. In this case, metal ions solution (50 mL of 100 mg·L⁻¹) was mixed thoroughly with KIT-6-

SO₃H (4.0 mg) and the supernatant concentration was measured by UV-Vis absorption spectroscopy at

different time intervals.

The linear plots of log (Q_e-Q_t) versus t and (t/Q_t) *versus* t were plotted for pseudo-first order and

pseudo-second-order models, respectively (Figure 7(a)&(b)). The rate constants k_1 and k_2 was calculated

from the slopes of the linear regressions. The rate constants, the correlation coefficients (R^2), and the

17

calculated Q_e for the adsorptive removal of metal ions by KIT-6-SO₃H are summarized in Table 2. Clearly, the R^2s of the pseudo-first-order model for Pb(II), Cd(II) and Cs(I) ions are 0.9884, 0.9895 and 0.9659, respectively. In contrast, the R^2 of the pseudo-second-order model for Pb(II), Cd(II) and Cs(I) ions are 0.9996, 0.9981 and 0.9873, with good linearities, indicating the applicability of the pseudo-second-order equation. In addition, the calculated Q_e values from pseudo-first-order model for the adsorptive removal of Pb(II), Cd(II) and Cs(I) ions by KIT-6-SO₃H are 79.51 mg·g⁻¹, 75.66 mg·g⁻¹ and 58.34 mg·g⁻¹, respectively. Further, in case of pseudo-second-order model, the calculated Q_e values are 100.75 mg·g⁻¹, 95.23 mg·g⁻¹ and 77.42 mg·g⁻¹, demonstrating the fitting of experimental data with pseudo-second-order model.
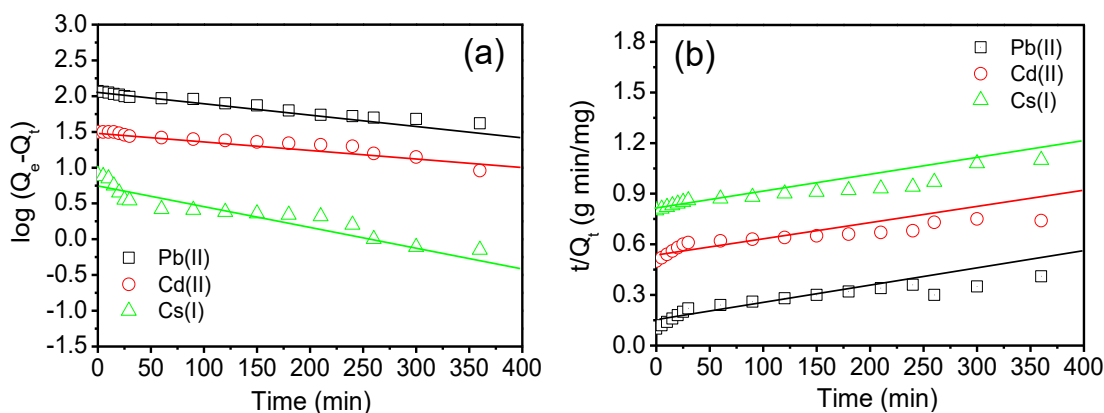

Figure 7. Fitting of adsorption kinetics of Pb(II), Cd(II) and Cs(I) ions into KIT-6-SO₃H using (a) Pseudo-first order model, (b) pseudo-second-order model.

Table 2. Summary of rate constants, correlation coefficients, and Q_e for adsorption of Pb(II), Cd(II) and Cs(I) ions into KIT-6-SO₃H.

Metal ion Kinetic model		Pb(II)	Cd(II)	Cs(I)
Pseudo-first order model	Q_e (mg·g⁻¹)	82.423	77.511	61.454
	K_1 (min⁻¹)	8.0332	6.0523	5.0262
	R^2	0.9887	0.9898	0.9669

18

Pseudo-second order model	Q_e (mg·g^{-1})	105.55	97.523	81.320
	K_2 (g·mg^{-1}·min^{-1})	17.036	14.041	12.062
	R^2	0.9999	0.9987	0.9876
Intraparticle diffusion model	K_i (mg·g^{-1}·min^{-1})	4.6236	4.4021	2.7141
	C (mg·g^{-1})	41.432	24.543	9.8670
	R^2	0.9894	0.9883	0.9827

Further, intraparticle diffusion model was fitted for modeling adsorption behavior occurs in a porous adsorbent. Intraparticle diffusion is a rate-controlling factor, uptake of the adsorbate varies with the square root of time. According to Eq. 7, the experimental data was analyzed, the plot of Q_t against $t^{1/2}$ gives a non-regression coefficient (Figure 8). As shown in Figure 8, within the first 5 mins, a linear graph could be plotted, corresponding to the fast adsorption uptake of Pb(II), Cd(II) and Cs(I) ions by KIT-6-SO$_3$H. In addition, the linear regression does not pass-through origin, indicating that the uptake is dominated by the external surface adsorption rather than intraparticle diffusion process. After that, adsorption speeds up, reflecting nonconsecutive diffusion of metal ions into mesopores, then diffusion remains fairly constant when the mesopore volumes are totally exhausted. It is well-known that adsorption controlled by the intraparticle diffusion model is favorable due to adsorption of metal ions inside the mesopores of a porous adsorbent [72]. From Figure 8, the intercepts of linear plots are 7.32 mg·g^{-1}, 4.43 mg·g^{-1} and 2.75 mg·g^{-1} for Pb(II), Cd(II) and Cs(I) ions, respectively. Disregarding the linearity (high R^2 value) of the intraparticle diffusion plots, the deviation of the line from the origin further reveals that intraparticle transport of metal ions through the mesopores of KIT-6-SO$_3$H is not only the rate-limiting mechanism, but also interaction with the active sites (–SO$_3$H) might be responsible for the adsorption process [73]. Thus, surface adsorption and intraparticle diffusion were likely to take place simultaneously.
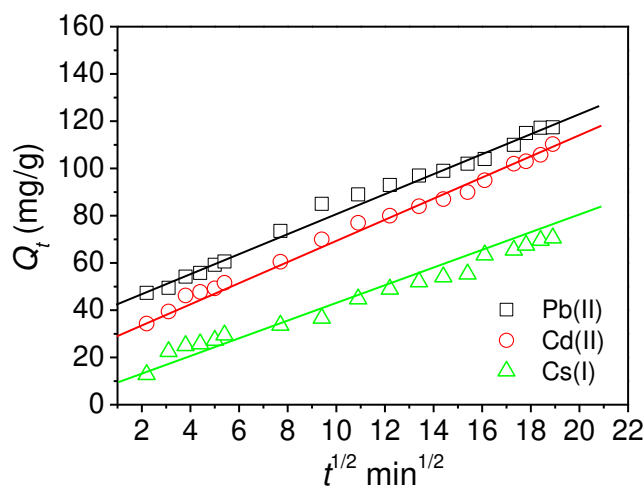
Figure 8. Intraparticle diffusion kinetic plot for the adsorption of Pb(II), Cd(II) and Cs(I) ions into the functionalized mesoporous silica KIT-6-SO₃H.

3.2.3 Adsorption isotherms

Correlation of equilibrium data using either a theoretical or empirical equation is important for prediction of the adsorption extent. To study the adsorption process, equilibrium adsorption data were investigated using Langmuir, Freundlich and Temkin models [64]. Langmuir adsorption isotherm (Eq. 8) is extensively used for expressing the adsorption behavior of a chemical species from a liquid solution supposing that the adsorption occurs at homogeneous substrate, while Freundlich adsorption (Eq. 9) takes into consideration that most of surfaces are heterogeneous with adsorption sites of varying energies [74]. Based on Langmuir model, the linear plot of C_e/Q_e against C_e for the adsorption of Pb(II), Cd(II) and Cs(I) ions by KIT-6-SO₃H is shown in Figure 9(a). The values of R^2 for Pb(II), Cd(II) and Cs(I) ions are 0.9967, 0.9961 and 0.990, respectively (Table 3). The calculated Q_e values for the adsorption of Pb(II), Cd(II) and Cs(I) ions by functionalzied KIT-6-SO₃H are 123.56 mg·g⁻¹, 117.52 mg·g⁻¹ and 90.66 mg·g⁻¹, respectively. On the other hand, the Freundlich and Tempkin isotherm models were also discussed and evaluated. The rate constants, the R^2s, and the calculated Q_e are summarized in Table 3. Figure 9(b)&(c), the R^2 values of the Freundlich isotherm are 0.9901, 0.9921 and 0.9584 and Temkin isotherm are 0.9852, 0.9897 and 0.9881 for Pb(II), Cd(II) and Cs(I) ions, respectively. Thus, KIT-6-SO₃H follows Langmuir

20

isotherm and the applicability suggests the monolayer coverage of the metal ion on the surface of KIT-6-SO$_3$H; thus, can be effectively used as an efficient adsorbent in treatment of wastewaters containing toxic Pb(II), Cd(II) and Cs(I) ions. By contrast, the adsorption of metal ions by mesoporous KIT-6-SO$_3$H may not follow Freundlich and Temkin isotherms, probably due to a different adsorption mechanism.
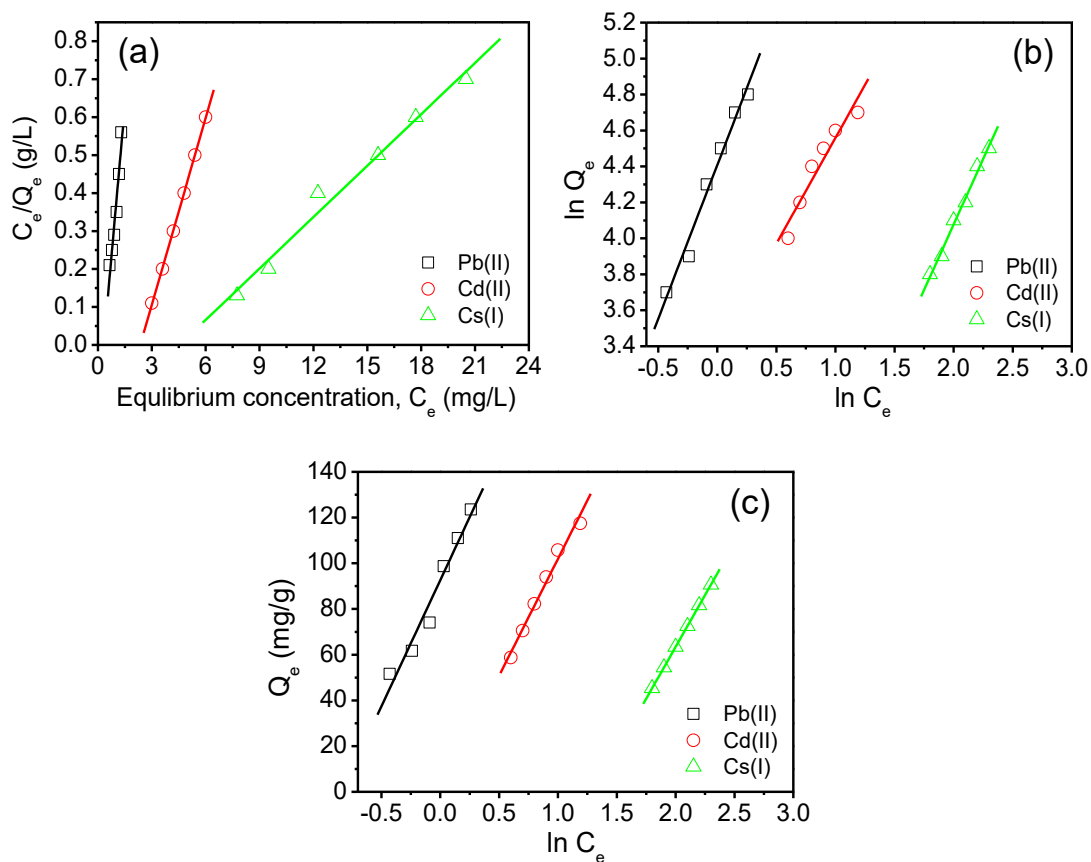

Figure 9. Fitting of adsorption isotherms of Pb(II), Cd(II) and Cs(I) ions into the functionalized mesoporous silica KIT-6-SO$_3$H (a) Langmuir model, (b) Freundlich model and (c) Temkin model, respectively.

Table 3. Summary of the fitted parameters in the Langmuir, Freundlich and Temkin isotherm models for adsorption of Pb(II), Cd(II) and Cs(I) ions into KIT-6-SO$_3$H.

Metal ion Isotherm models	Pb(II)	Cd(II)	Cs(I)

Langmuir isotherm	Q_e (mg·g^{-1})	123.56	117.52	90.66
	K_l (L·g^{-1})	3.8341	3.4182	0.846
	a_l (L·mg^{-1})	2.3835	2.3321	2.261
	R^2	0.9967	0.9961	0.990
Freundlich isotherm	K_f (L·g^{-1})	15.775	15.396	12.702
	n	0.6122	0.4832	0.3864
	R^2	0.9901	0.9921	0.9584
Temkin isotherm	K_t (L·mg^{-1})	33.754	25.813	23.146
	B	24.969	23.756	18.315
	R^2	0.9852	0.9897	0.9881

Interestingly, our functionalized mesoporous silica KIT-6-SO$_3$H with high surface area and large pore diameter exhibits a remarkable adsorption uptake for Pb(II), Cd(II) and Cs(I) ions, compared to those previously reported for functionalized mesoporous silicas, polymeric materials, carbon nanomaterials and Prussian blue (PB) (Table S1) [43,44,59,75–89]. The surface area might not be the main factor for the high adsorption affinity of functionalized KIT-6-SO$_3$H towards metal ions from aqueous solution, other function should be considered, as well.

4. Conclusion

Functionalized mesoporous silica KIT-6 with highly acidic –SO$_3$H groups was successfully realized through a controlled post-grafting method. Even after functionalization, mesoporous KIT-6-SO$_3$H still possess a high BET surface area. Applying the QCM sensor coated with KIT-6-SO$_3$H thin layers demonstrated that the functionalization of KIT-6 with acidic –SO$_3$H groups can be used as an efficient adsorbent for removal of Pb(II), Cd(II) and Cs(I) ions. Combing the unique properties such as high BET surface area and pore diameter induced by the 3D cubic mesostructure of KIT-6, as well as the active – SO$_3$H groups decorated the inner and outer pore wall surfaces facilitated a high diffusion uptake of metal ions inside the mesopores with a high adsorption capability. Our KIT-6-SO$_3$H showed an impressive

saturation capacity for Pb(II), Cd(II) and Cs(I) ions with good selectivity according to their K_a values. The metal ion adsorption kinetics were well-described by the surface reaction and diffusion controlled models. The adsorption behavior was found to obey a second-order kinetic and Langmuir isotherm models. We believe that functionalized mesoporous silica KIT-6-SO$_3$H integrated with a QCM sensor technique will be promising in a wide range of environmental remediation.

References

[1] Y. Pan, Z. Liu, W. Wang, C. Peng, K. Shi, X. Ji, Highly efficient macroporous adsorbents for toxic metal ions in water systems based on polyvinyl alcohol–formaldehyde sponges, J. Mater. Chem. A 4 (2016) 2537–2549.

[2] V. K. Gupta, P. J. M. Carrott, M. M. L. Ribeiro, Suhas. Low-cost adsorbents: Growing approach to wastewater treatment–a review, Crit. Rev. Environ. Sci. Technol. 39 (2009) 783−842.

[3] K. Huang, B. Li, F. Zhou, S. Mei, Y. Zhou, T. Jing, Selective solid-phase extraction of lead ions in water samples using three-dimensional ion-imprinted polymers, Anal. Chem. 88 (2016) 6820–6826.

[4] X. Wang, W. Liu, J. Tian, Z. Zhao, P. Hao, X. Kang, Y. Sang, H. Liu, Cr(VI) Pb(II) Cd(II) adsorption properties of nanostructured BiOBr microspheres and their application in a continuous filtering removal device for heavy metal ions, J. Mater. Chem. A 2 (2014) 2599–2608.

[5] J. Peterson, M. Macdonell, L. Haroun, F. R. Monette, R. D. Hildebr, A. Taboas, Human Health Fact Sheet (2005), Radiological and Chemical Fact Sheets to Support Health Risk Analyses for Contaminated Areas, Argonne National Laboratory Environmental Science Divisions, (2007).

[6] N. L. Torad, M. Hu, M. Imura, M. Naito, Y. Yamauchi, Large Cs adsorption capability of nanostructured Prussian Blue particles with high accessible surface areas, J. Mater. Chem. 22 (2012) 18261–18267.

[7] B. Zou, K. Chen, Y. Wang, C. Niu, S. Zhou, Amino-functionalized magnetic magnesium silicate double-shelled hollow microspheres for enhanced removal of lead ions, RSC Adv. 5 (2015) 22973–22979.

[8] WHO, Guidelines for drinking-water quality, 4th ed., WHO Press, Geneva, (2011).

[9] L. Zhang, M. Fang, Nanomaterials in pollution trace detection and environmental improvement, Nano Today 5 (2010) 128–142.

[10] S. Wei, Y. Liu, S. Shao, L. Liu, H. Wang, Y. Liu, Preparation of magnetic Pb(II) and Cd(II) ion-imprinted microspheres and their application in determining the Pb(II) and Cd(II) contents of environmental and food samples, RSC Adv. 4 (2014) 29715–29723.

[11] A. A. Ensafi, Z. N. Isfahani, A simple optical sensor for cadmium ions assay in water samples using spectrophotometry, J. Anal. Chem. 66 (2011) 151–157.

[12] US Environmental Protection Agency, Integrated Risk Information System (IRIS) on Cadmium, National Center for Environmental Assessment, Office of Research and Development, Washington, DC, (1999).

[13] E. G. Segura, M. S. Ríos, A. C. Cruz, C. Fall, Adsorption of cadmium by Na and Fe modified zeolitic tuffs and carbonaceous material from pyrolyzed sewage sludge, J. Environ. Manage. 97 (2012) 6–13.

[14] Y. Guo, Y. Zhang, H. Shao, Z. Wang, X. Wang, X. Jiang, Label-free colorimetric detection of cadmium ions in rice samples using gold nanoparticles, Anal. Chem. 86 (2014) 8530–8534.

[15] M. Garmsiri, H. R. Mortaheb, Enhancing performance of hybrid liquid membrane process supported by porous anionic exchange membranes for removal of cadmium from wastewater, Chem. Eng. J. 264 (2015) 241–250.

[16] S. Bayar, A. E. Yilmaz, R. Boncukcuoglu, B. A. Fil, M. M. Kocakerim, Effects of operational parameters on cadmium removal from aqueous solutions by electrochemical coagulation, Desalin. Water Treat. 51 (2013) 2635–2643.

[17] G. Liu, Y. Zhang, M. Qia, F. Chen, Covalent anchoring of multifunctionized gold nanoparticles on electrodes towards an electrochemical sensor for the detection of cadmium ions, Anal. Methods 7 (2015) 5619–5626.

[18] M. R. Mahmoud, N. K. Lazaridis, K. A. Matis, Study of flotation conditions for cadmium(II) removal from aqueous solutions, Process Saf. Environ. Prot. 94 (2015) 203–211.

[19] M. G. S. Martínez, E. L. Silva, R. Encalada, E. Pineda, J. C. G. Pérez, A. Z. Rodriguez, R. M. Sánchez, E. Saavedra, R. J. Chávez, Cadmium removal by Euglena gracilis is enhanced under anaerobic growth conditions, J. Hazard. Mater. 288 (2015) 104–112.

[20] S. Vasudevan, J. Lakshmi, G. Sozhan, Effects of alternating and direct current in electrocoagulation process on the removal of cadmium from water, J. Hazard. Mater. 192 (2011) 26–34.

[21] M. J. Manos, M. G. Kanatzidis, Metal sulfide ion exchangers: Superior sorbents for the capture of toxic and nuclear waste-related metal ions, Chem. Sci. 7 (2016) 4804–4824.

[22] M. Paul, N. Pal, P. R. Rajamohanan, B. S. Rana, A. K. Sinha, A. Bhaumik, New organic–inorganic hybrid microporous organosilica having high metal ion adsorption capacity, Phys. Chem. Chem. Phys. 12 (2010) 9389–9394.

[23] S. S. Gupta, K. G. Bhattacharyya, Adsorption of metal ions by clays and inorganic solids, RSC Adv. 4 (2014) 28537–28586.

[24] Z.-Q. Zhao, X. Chen, Q. Yang, J.-H. Liu, X.-J. Huang, Selective adsorption toward toxic metal ions results in selective response: electrochemical studies on a polypyrrole/reduced graphene oxide nanocomposite, Chem. Commun. 48 (2012) 2180–2182.

[25] D. P. Quintanilla, I. d. Hierro, M. Fajardo, I. Sierra, Adsorption of cadmium(II) from aqueous media onto a mesoporous silica chemically modified with 2-mercaptopyrimidine, J. Mater. Chem. 16 (2006) 1757–1764.

[26] J. C. Izidoro, D. A. Fungaro, J. E. Abbott, S. Wang, Synthesis of zeolites X and A from fly ashes for cadmium and zinc removal from aqueous solutions in single and binary ion systems, Fuel 103 (2013) 827–834.

[27] T. M. Alslaibi, I. Abustan, M. A. Ahmad, A. A. Foul, Cadmium removal from aqueous solution using microwaved olive stone activated carbon, J. Environ. Chem. Eng. 1 (2013) 589–599.

[28] B. Xiao, K. M. Thomas, Competitive adsorption of aqueous metal ions on an oxidized nanoporous activated carbon, Langmuir 20 (2004) 4566–4578.

[29] K. Huang, B. Li, F. Zhou, S. Mei, Y. Zhou, T. Jing, Selective solid-phase extraction of lead ions in water samples using three-dimensional ion-imprinted polymers, Anal. Chem. 88 (2016) 6820–6826.

[30] S. Wei, Y. Liu, M. Shao, L. Liu, H. Wang, Y. Liu, Preparation of magnetic Pb(II) and Cd(II) ion-imprinted microspheres and their application in determining the Pb(II) and Cd(II) contents of environmental and food samples, RSC Adv. 4 (2014) 29715–29723.

[31] V. K. Gupta, S. Sharma, Removal of cadmium and zinc from aqueous solutions using Red mud, Environ. Sci. Technol. 36 (2002) 3612–3617.

[32] L. Huang, S. Yuan, L. Lv, G. Tan, B. Liang, S. O. Pehkonen, Poly(methacrylic acid)-grafted chitosan microspheres via surface-initiated ATRP for enhanced removal of Cd(II) ions from aqueous solution, J. Colloid Interface Sci. 405 (2013) 171–182.

[33] L.-Y. Wang, M.-J. Wang, emoval of heavy metal ions by poly(vinyl alcohol) and carboxymethyl cellulose composite hydrogels prepared by a freeze–thaw method, ACS Sustainable Chem. Eng. 4 (2016) 2830–2837.

[34] L. Ma, Q. Wang, S. M. Islam, Y. Liu, S. Ma, M. G. Kanatzidis, Highly selective and efficient removal of heavy metals by layered double hydroxide intercalated with the MoS_4^{2-} Ion, J. Am. Chem. Soc. 138 (2016) 2858–2866.

[35] D. Vilela, J. Parmar, Y. Zeng, Y. Zhao, S. Sánchez, Graphene-based microbots for toxic heavy metal removal and recovery from water, Nano Lett. 16 (2016) 2860–2866.

[36] Y. Wang, J. Hu, Q. Zhuang, Y. Ni, Label-free fluorescence sensing of lead(II) ions and sulfide ions based on luminescent molybdenum disulfide nanosheets, ACS Sustainable Chem. Eng. 4 (2016) 2535–2541.

[37] S. Bao, Y. Li, Z. Fei, H. Mei, Y. Zhou, X. Wang, D. Liu, Effective adsorption of uranium(VI) from aqueous solution using ethylene-bridged mesoporous silica functionalized with ureido groups, J. Radioanal. Nucl. Chem. 324 (2020) 385–394.

[38] W. Zhu, J. Wang, D. Wu, X. Li, Y. Luo, C. Han, W. Ma, S. He, Investigating the heavy metal adsorption of mesoporous silica materials prepared by microwave synthesis, Nanoscale Res. Lett. 12 (2017) 323.

[39] S. Jahan, M. Salman, Y. B. Alias, A. F. B. A. Bakar, F. Mansoore, S. Kanwal, Polymer-modified mesoporous silica microcubes (P@MSMCs) for the synergistic oxidative entrapment of Ag(i), Ti(iv), and Zn(ii) from natural river water. Dalton Trans. 49 (2020) 8265–8273.

[40] J.-Y. Lee, C.-H. Chen, S. Cheng, H.-Y. Li, Adsorption of Pb(II) and Cu(II) metal ions on functionalized large-pore mesoporous silica, Int. J. Environ. Sci. Technol. 13 (2016) 65–76.

[41] J. G. Croissant X. Cattoën, M. W. Chi Man, J.-O. Durand, N. M. Khashab, Syntheses and applications of periodic mesoporous organosilica nanoparticles, Nanoscale 7 (2015) 20318–20334.

[42] Y. Zhang, L. Ding, W. Zhao, Y. Zhang, F. Han, Q. Feng, J. Song, M. Li, B. Dua, Q. Wei, Hydrophobic bifunctionalized hexagonal mesoporous silicas as efficient adsorbents for the removal of Orange IV, RSC Adv. 4 (2014) 49783–49788.

[43] J. M. Arsuaga, J. Aguado, A. Arencibia, M. S. López-Gutiérrez, Aqueous mercury adsorption in a fixed bed column of thiol functionalized mesoporous silica, Adsorption 20 (2014) 311–319.

[44] M. C. Bruzzoniti, A. Prelle, C. Sarzanini, B. Onida, S. Fiorilli, E. Garrone, Retention of heavy metal ions on SBA-15 mesoporous silica functionalized with carboxylic groups, J. Sep. Sci. 30 (2007) 2414–2420.

[45] T. Yokoi, H. Yoshitake, T. Tatsumi, Synthesis of amino-functionalized MCM-41 via direct co-condensation and post-synthesis grafting methods using mono- di- and tri-amino-organoalkoxysilanes, J. Mater. Chem. 14 (2004) 951–957.

[46] J. I. Lachowicz, A.-H. Emwas, G. R. Delpiano, A. Salis, M. Piludu, L. Jaremko, M. Jaremko, Metal coordination: Improving metal adsorption on triethylenetetramine (TETA) functionalized SBA-15 mesoporous silica using potentiometry, EPR and ssNMR. Adv. Mater. Interfaces 7 (2020) 2070082.

[47] R. Gupta, S. K. Gupta, D. D. Pathak, Selective adsorption of toxic heavy metal ions using guanine-functionalized mesoporous silica [SBA-16-g] from aqueous solution, Micropor. Mesopor. Mater. 288 (2019) 109577.

[48] E.-H. Jang, S. P. Pack, I. Kim, S. Chung, A systematic study of hexavalent chromium adsorption and removal from aqueous environments using chemically functionalized amorphous and mesoporous silica nanoparticles, Sci. Rep. 10 (2020) 5558.

[49] X. Chen, W. K. Ching, K. F. Lam, W. Wei, K. L. Yeung, An investigation of the selective adsorptions of metals on mesoporous NH_2-MCM-41, J. Phys. Chem. C 120 (2016) 18365–18376.

[50] C. Gunathilake, M. S. Kadanapitiye, O. Dudarko, S. D. Huang, M. Jaroniec, Adsorption of lead ions from aqueous phase on mesoporous silica with P-containing pendant groups, ACS Appl. Mater. Interfaces 7 (2015) 23144–23152.

[51] M. Anbia, K. Kargosha, S. Khoshbooei, Heavy metal ions removal from aqueous media by modified magnetic mesoporous silica MCM-48, Chem. Eng. Res. Des. 93 (2015) 779–788.

[52] M. Mureseanu, A. Reiss, I. Stefanescu, E. David, V. Parvulescu, G. Renard, V. Hulea, Modified SBA-15 mesoporous silica for heavy metal ions remediation, Chemosphere 73 (2008) 1499–1504.

[53] A. M. Rabie, H. M. Abd El-Salam, M. A. Betiha, H. H. El-Maghrabi, D. Aman, Mercury removal from aqueous solution *via* functionalized mesoporous silica nanoparticles with the amine compound, Egypt. J. Pet. 28 (2019) 289–296.

[54] J. Wei, S. Chen, Y. Li, Z. He, L. Geng, L. Liao, Aqueous Cu(ii) ion adsorption by amino-functionalized mesoporous silica KIT-6, SC Adv. 10 (2020) 20504–20514.

[55] S. Shariati, M. Khabazipour, F. Safa, Synthesis and application of amine functionalized silica mesoporous magnetite nanoparticles for removal of chromium (VI) from aqueous solutions, J. Porous Mater. 24(1) (2017) 129–139.

[56] M. Sojoudi, S. Shariati, M. Khabazipour, Amine functionalized KIT-6 mesoporous magnetite nanocomposite as an efficient adsorbent for removal of Ponceau 4R dye from aqueous solutions, Analyt. Bioanalyt. Chem. Res. 3(2) (2016) 287–298.

[57] L. Zhu, X. Shi, L. Song, Y. Sun, S. Chen, W. Wu, Mesoporous silica (KIT-6) derivatized with hydroxyquinoline functionalities as a selective adsorbent of uranium(VI), J. Radioanal. Nucl. Chem. 308 (2016) 381–392.

[58] Z. Ezzeddine, I. Batonneau-Gener, Y. Pouilloux, H. Hamad, Z. Saad, V. Kazpard, Divalent heavy metals adsorption onto different types of EDTA-modified mesoporous materials: Effectiveness and complexation rate, Micropor. Mesopor. Mater. 212 (2015) 125–136.

[59] N. Bensacia, I. Fechete, S. Moulay, O. Hulea, A. Boos, F. Garin, Kinetic and equilibrium studies of lead(II) adsorption from aqueous media by KIT-6 mesoporous silica functionalized with –COOH, C. R. Chimie 17 (2014) 869–880.

[60] M. M. Ayad, N. A. Salahuddin, N. L. Torad, A. A. El-Nasr, pH-Responsive sulphonated mesoporous silica: a comparative drug release study, RSC Adv. 6 (2016) 57929–57940.

[61] P. W. Atkins, Physical Chemistry, Oxford University Press, Oxford, 2nd edn. (1982), p. 1023.

[62] G. Sauerbrey, Verwendung von Schwingquarzen zur Wägung dünner Schichten und zur Mikrowägung, Z. Phys. 155 (1959) 206–222.

[63] W. J. Weber, J. C. J. Morris, Kinetics of adsorption of carbon from solution, Sanit. Eng. Di V., Am. Soc. Ci V. Eng. 89 (1963) 31–59.

[64] I. Langmuir, The adsorption of gases on plane surfaces of glass mica and platinum, J. Am. Chem. Soc. 40 (1918) 1361–1403.

[65] N. L. Torad, J. Kim, M. Kim, H. Lim, J. Na, S. M. Alshehri, T. Ahamad, Y. Yamauchi, M. Eguchi, B. Ding, X. Zhang, Nanoarchitectured porous carbons derived from ZIFs toward highly sensitive and selective QCM sensor for hazardous aromatic vapors, J. Hazard. Mater. 405 (2020) 124248.

[66] S. Zhang, J. Wang, N. L. Torad, W. Xia, M. A. Aslam, Y. V. Kaneti, Z. Hou, Z. Ding, B. Da, A. Fatehmulla, A. M. Aldhafiri, W. A. Farooq, J. Tang, Y. Bando, and Y. Yamauchi, Rational design of nanoporous MoS_2/VS_2 heteroarchitecture for ultrahigh performance ammonia sensors, Small 16 (2020) 1901718.

[67] N. L. Torad, S. Zhang, W. A. Amer, M. M. Ayad, M. Kim, J. Kim, B. Ding, X. Zhang, T. Kimura, Y. Yamauchi, Advanced nanoporous material based QCM devices: A new horizon of interfacial mass sensing technology, Adv. Mater. Interfaces 6 (2019) 1900849.

[68] M. M. Ayad, N. A. Salahuddin, A. A. El-Nasr, N. L. Torad, Amine-functionalized mesoporous silica KIT-6 as a controlled release drug delivery carrier, Micropor. Mesopor. Mater. 229 (2016) 166–177.

[69] I. A. Sengil, M. Özacar, Competitive biosorption of Pb^{2+} Cu^{2+} and Zn^{2+} ions from aqueous solutions onto valonia tannin resin, J. Hazard. Mater. 166 (2009) 1488–1494.

[70] N. Bakhtiari, S. Azizian, N. L. Torad, Y. Yamauchi, Study on adsorption of copper ion from aqueous solution by MOF-derived nanoporous carbon, Micropor. Mespor. Mater. 217 (2015) 173–177.

[71] X. Wang, W. Cai, Y. Lin, G. Wang, C. Liang, Mass production of micro/nanostructured porous ZnO plates and their strong structurally enhanced and selective adsorption performance for environmental remediation, J. Mater. Chem. 20 (2010) 8582–8590.

[72] B. Ji, F. Shao, G. Hu, S. Zheng, Q. Zhang, Z. Xu, Adsorption of methyl tert-butyl ether (MTBE) from aqueous solution by porous polymeric adsorbents, J. Hazard. Mater. 161 (2009) 81–87.

[73] B. H. Hameed, Evaluation of papaya seeds as a novel non-conventional low-cost adsorbent for removal of methylene blue, J. Hazard. Mater. 162 (2009) 939–944.

[74] I. Langmuir, The constitution and fundamental properties of solids and liquids. Part I solids, J. Am. Chem. Soc. 38 (1916) 2221–2295.

[75] A. Heidari, H. Younesi, Z. Mehraban, Removal of Ni(II) Cd(II) and Pb(II) from a ternary aqueous solution by amino functionalized mesoporous and nano mesoporous silica, Chem. Eng. J. 153 (2009) 70–79.

[76] K.F. Lam, K.L. Yeung, G. McKay, Efficient approach for Cd^{2+} and Ni^{2+} removal and recovery using mesoporous adsorbent with tunable selectivity, Environ. Sci. Technol. 41 (2007) 3329–3334.

[77] A. Shahbazi, H. Younesi, A. Badiei, Functionalized SBA-15 mesoporous silica by melamine-based dendrimer amines for adsorptive characteristics of Pb(II) Cu(II) and Cd(II) heavy metal ions in batch and fixed bed column, Chem. Eng. J. 168 (2011) 505–518.

[78] I. Georgescu, M. Mureşeanu G. C. V. Hulea, Adsorptive removal of cadmium and copper from water by mesoporous silica functionalized with N-(aminothioxomethyl)-2-thiophen carboxamide, J. Environ. Eng. 139 (2013) 1285–1296.

[79] D. Pérez-Quintanilla, I. D. Hierro, M. Fajardo, I. Sierra, Adsorption of cadmium(II) from aqueous media onto a mesoporous silica chemically modified with 2-mercaptopyrimidine, J. Mater. Chem. 16 (2006) 1757–1764.

[80] B. Gao, Y. Gao, Y. Li, Preparation and chelation adsorption property of composite chelating material poly(amidoxime)/SiO2 towards heavy metal ions, Chem. Eng. J. 158 (2010) 542–549.

[81] S. Venkateswarlu, M. Yoon, Rapid removal of cadmium ions using green-synthesized Fe_3O_4 nanoparticles capped with diethyl-4-(4 amino-5-mercapto-4H-124-triazol-3-yl)phenyl phosphonate, RSC Adv. 5 (2015) 65444–65453.

[82] R. Karthik, S. Meenakshi, Removal of Pb(II) and Cd(II) ions from aqueous solution using polyaniline grafted chitosan, Chem. Eng. J. 263 (2015) 168–177.

[83] R. Hua, Z. Li, Sulfhydryl functionalized hydrogel with magnetism: Synthesis characterization and adsorption behavior study for heavy metal removal, Chem. Eng. J. 249 (2014) 189–200.

[84] L. Vitali, M. C. M. Laranjeira, N. S. Goncalves, V. T. Favere, Spray-dried chitosan microspheres containing 8-hydroxyquinoline -5 sulphonic acid as a new adsorbent for Cd(II) and Zn(II) ions, Int. J. Biol. Macromol. 42 (2008) 152–157.

[85] Z. Li, H. Fan, Y. Zhang, M. Chen, Z. Yu, X. Cao, T. Sun, Cd(II)-imprinted polymer sorbents prepared by combination of surface imprinting technique with hydrothermal assisted sol-gel process for selective removal of cadmium(II) from aqueous solution, Chem. Eng. J. 171 (2011) 703–710.

[86] M. Behbahania, A. Bagheri, M. Taghizadeh, M. Salarian, O. Sadeghi, L. Adlnasab, K. Jalali, Synthesis and characterisation of nano structure lead (II) ion-imprinted polymer as a new sorbent for selective extraction and preconcentration of ultra-trace amounts of lead ions from vegetables rice and fish samples, Food Chem. 138 (2013) 2050–2056.

[87] M. Tuzen, K. O. Saygi, M. Soylak, Solid phase extraction of heavy metal ions in environmental samples on multiwalled carbon nanotubes, J. Hazard. Mater. 152 (2008) 632–639.

[88] S. Z. Mohammadi, D. Afzali, D. Pourtalebi, Flame atomic absorption spectrometric determination of trace amounts of lead cadmium and nickel in different matrixes after solid phase extraction on modified multiwalled carbon nanotubes, Cent. Eur. J. Chem. 3 (2010) 662–668.

[89] Z. Li, L. Wu, Synthesis characterization and application of 4-aminoazobenzene functionalized multiwalled carbon nanotubes as a novel and uniquely selective solid-phase extraction for determination of lead(II) in water samples, Int. J. Environ. Anal. Chem. 94 (2014) 291–303.

TOC image
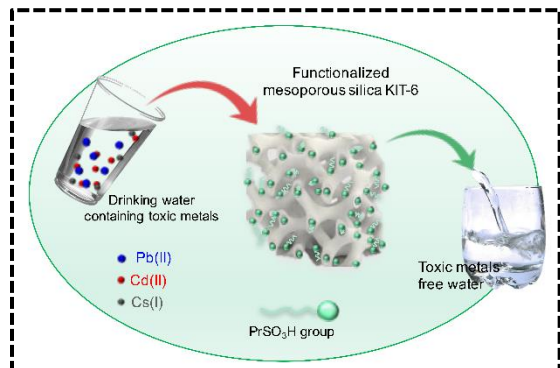
Adsorption study of toxic metal ions using functionalized 3D mesostructured silica

Nagy L. Torad, Ahmed Abu El-Nasr, Nehal A. Salahuddin, Mohamad M. Ayad

Figures
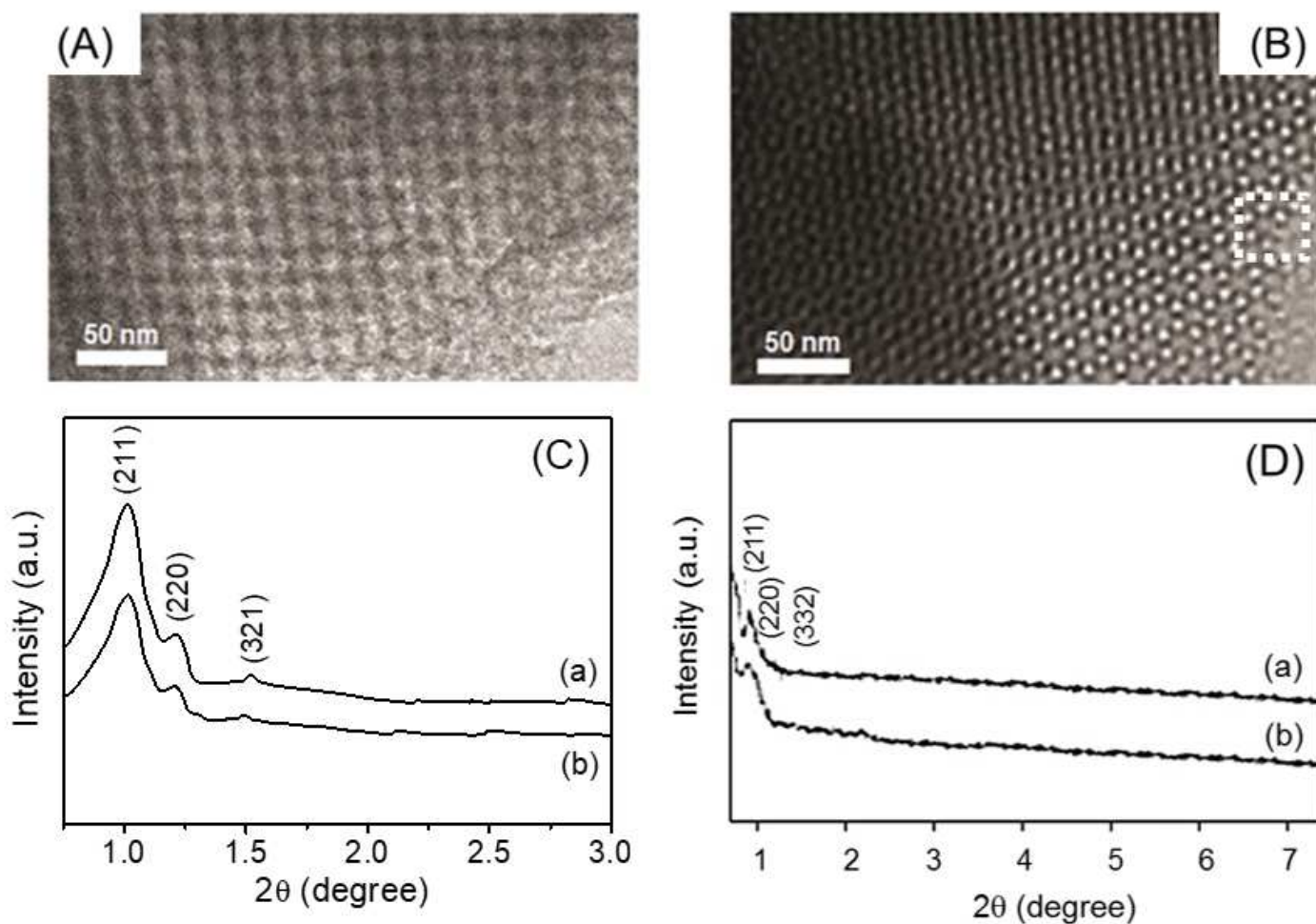
Figure 1

(A&B) TEM images of pristin mesoporous silica KIT-6 and functionalized KIT-6-SO3H, respectively. TEM image of the original KIT-6 and KIT-6-SO3H ((Ia3 ̄d) space group) taken with the incident beam parallel to the [111] direction. (C&D) small-angle SAXS measurements and low-angle XRD patterns of (a) KIT-6 and (b) KIT-6-SO3H, respectively.
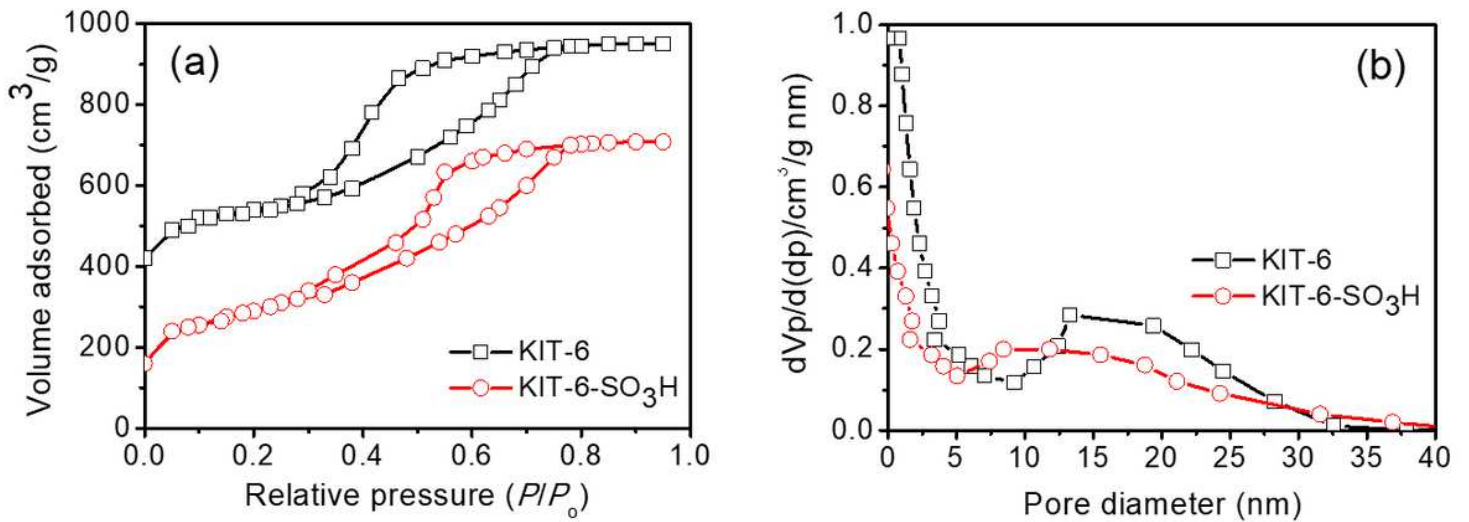
Figure 2

(a & b) Nitrogen adsorption-desorption isotherms and pore size distributions of pristin mesoporous silica KIT-6 (black line) and functionalized mesoporous KIT-6-SO3H (red line).
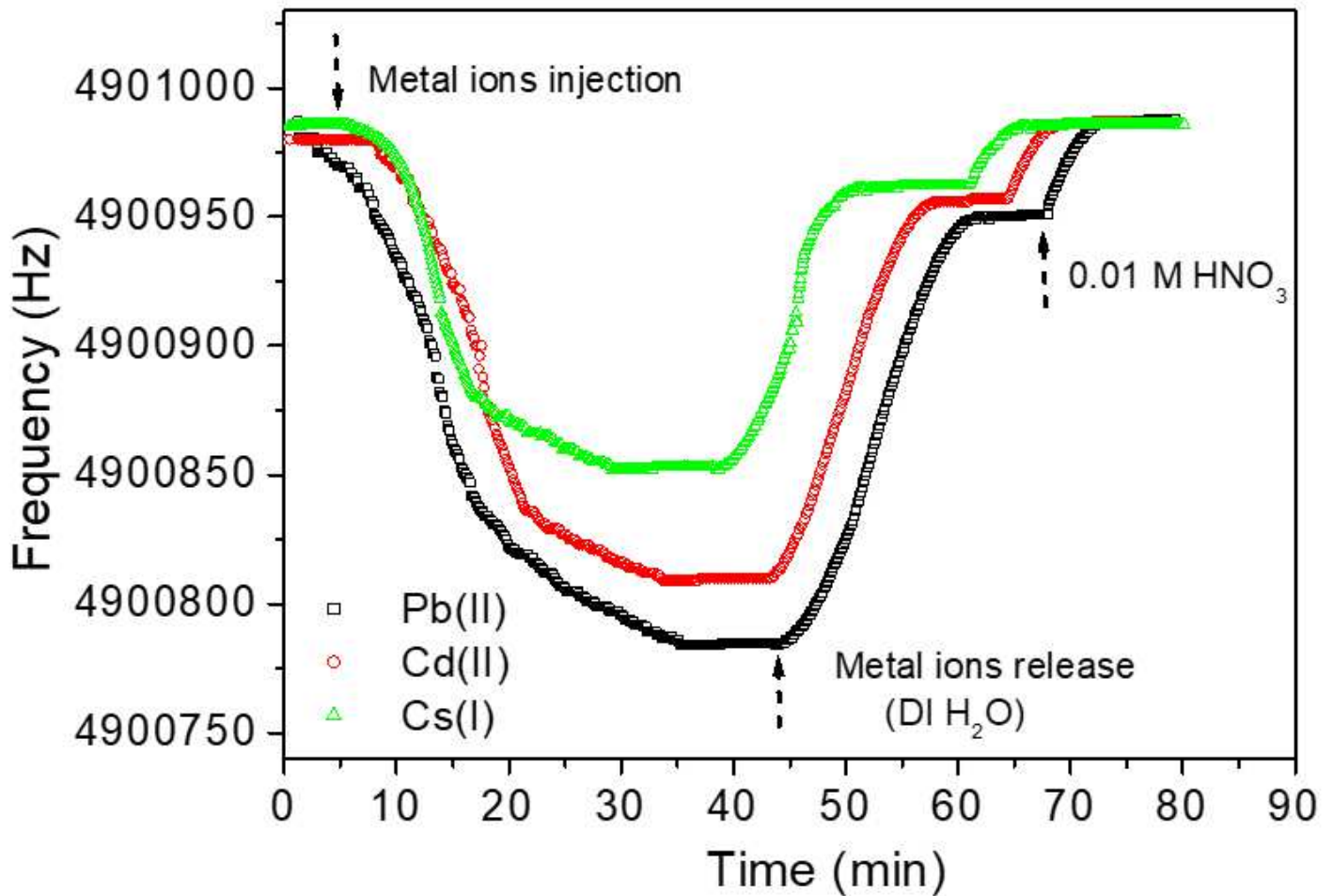
Figure 3

Mass-normalized time-dependence frequency shifts of QCM electrodes coated with KIT-6-SO3H upon exposure to Pb(II), Cd(II) and Cs(I) ions solutions (after the injection of metals ions solutions (10 ppmv, 10 mL). Release test of Pb(II), Cd(II) and Cs(I) ions was conducted by addition of DI H2O into the QCM electrode followed by addition of 0.01 M HNO3.
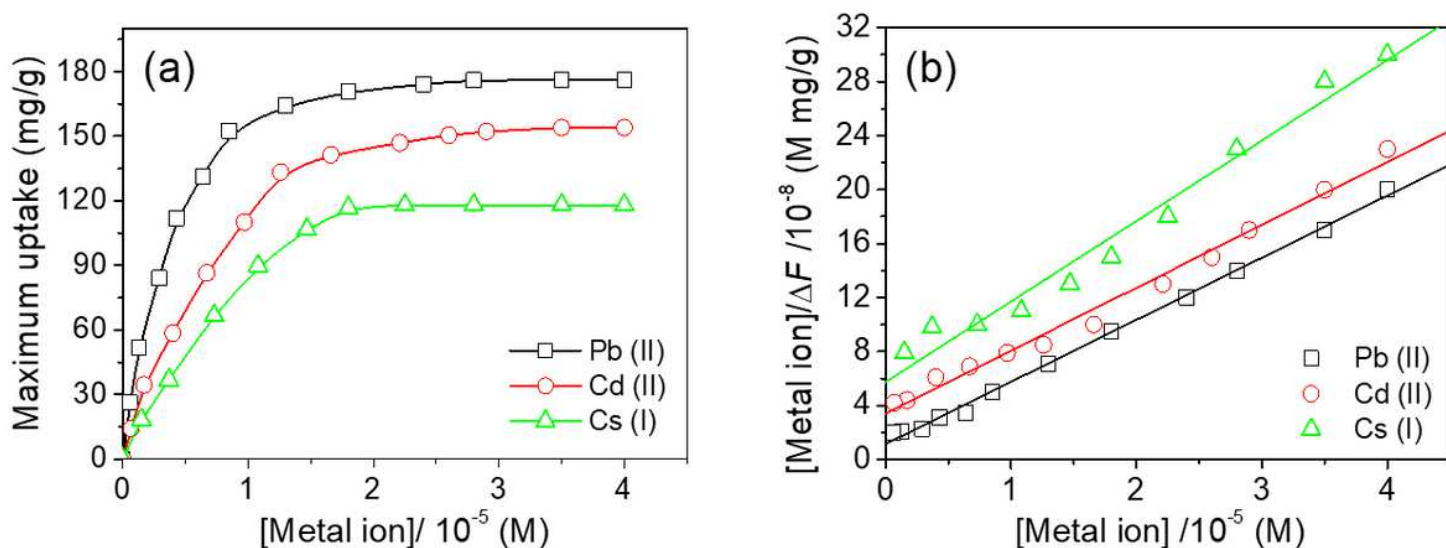
Figure 4

(a) Saturation binding behaviors of Pb(II), Cd(II) and Cs(I) ions depending on concentrations of metal ions at 25 °C. (b) Their linear reciprocal plots of [Metal ion]/ΔF against [Metal ion].
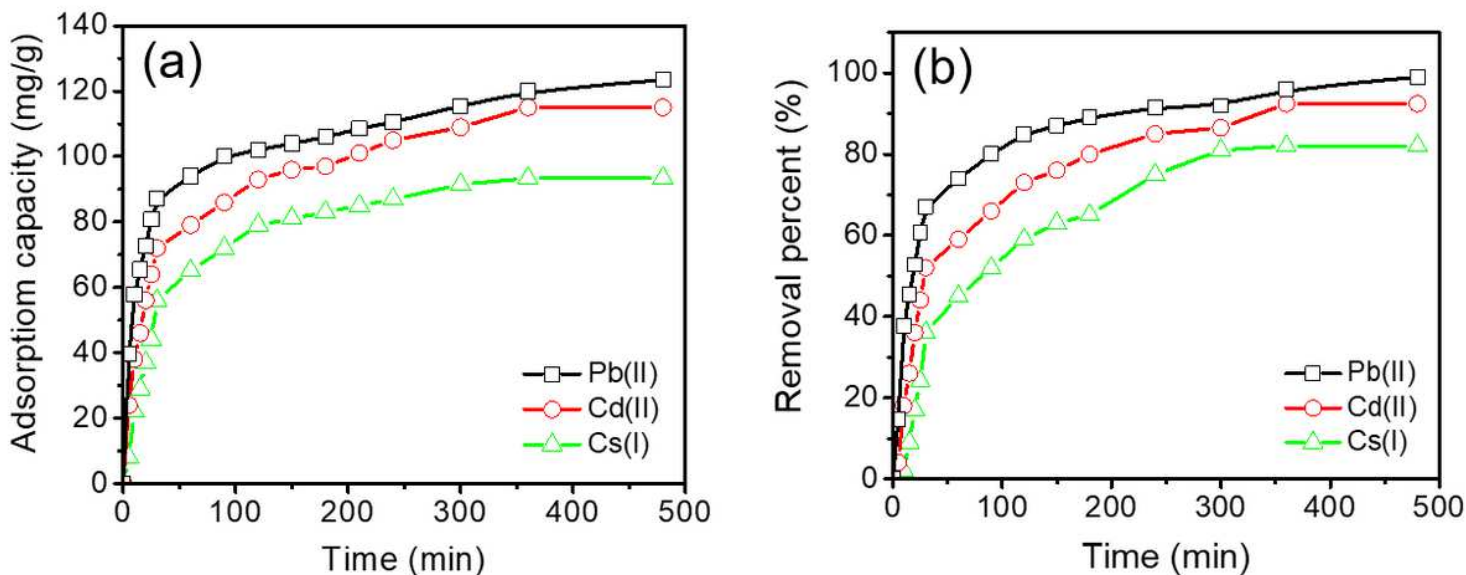
Figure 5

(a) Time-dependent adsorption capacities and (b) removal efficacy of KIT-6-SO3H toward Pb(II), Cd(II) and Cs(I) ions (100 ppmv).
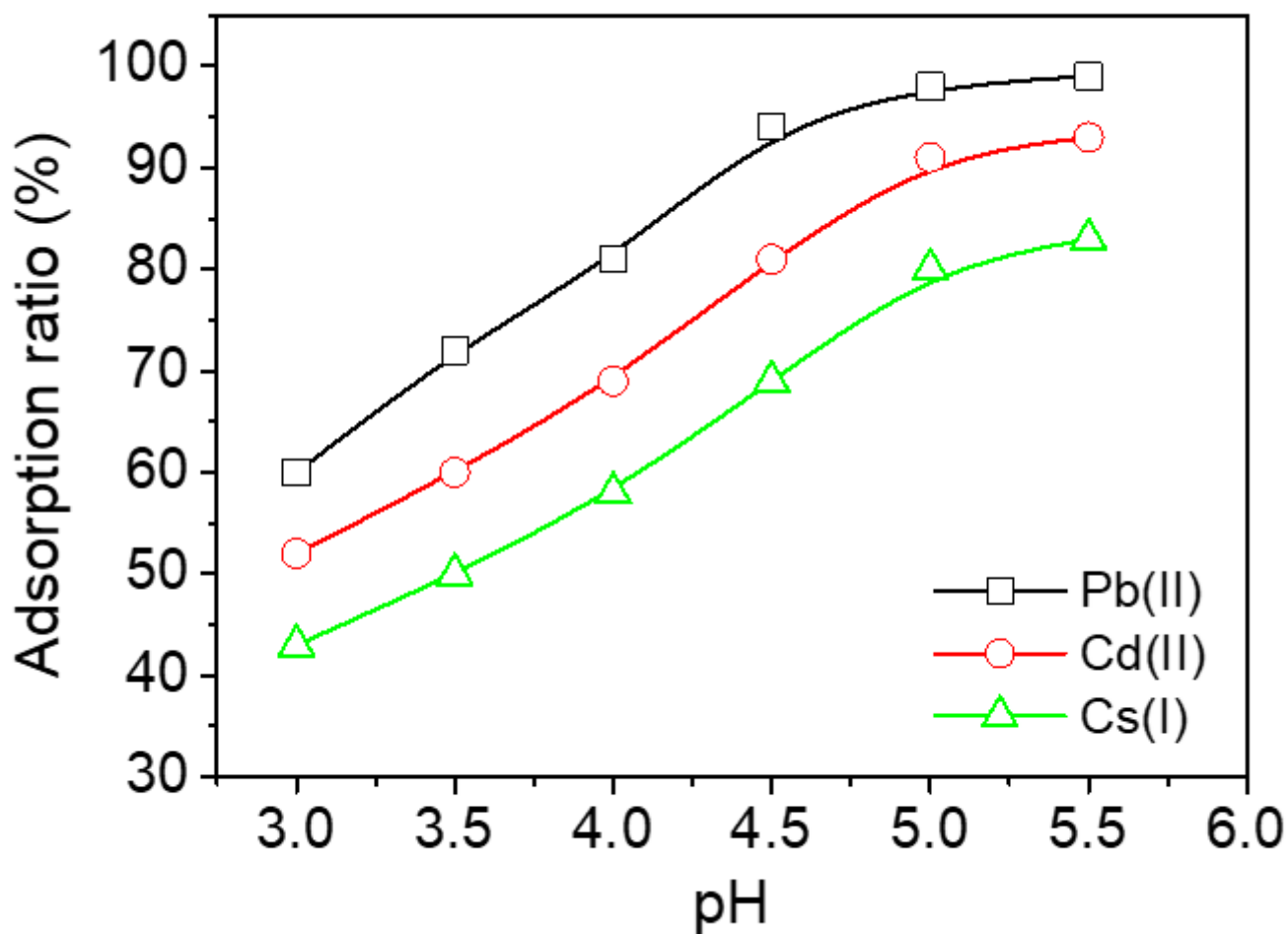
Figure 6

The effect of pH on the removal percentage of Pb(II), Cd(II) and Cs(I) ions by functionalized mesoporous silica KIT-6-SO3H.
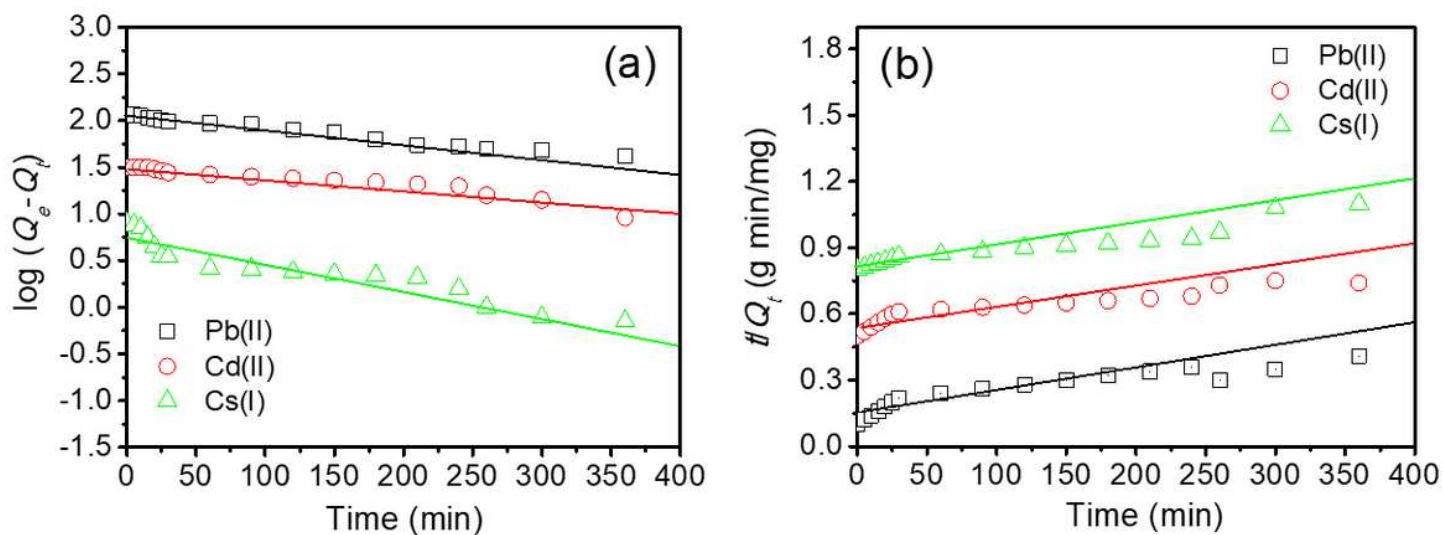
Figure 7

Fitting of adsorption kinetics of Pb(II), Cd(II) and Cs(I) ions into KIT-6-SO3H using (a) Pseudo-first order model, (b) pseudo-second-order model.
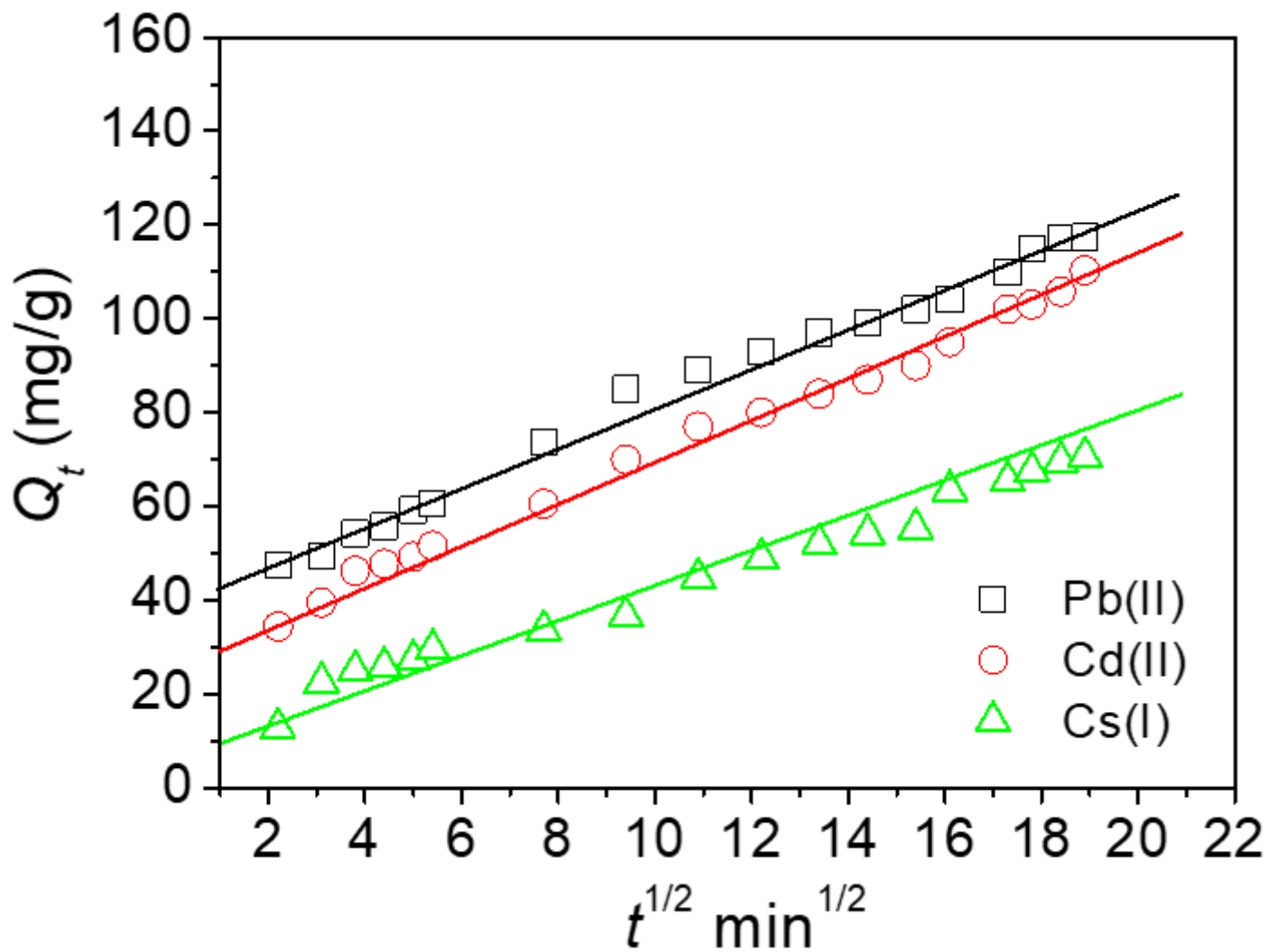

Figure 8

Intraparticle diffusion kinetic plot for the adsorption of Pb(II), Cd(II) and Cs(I) ions into the functionalized mesoporous silica KIT-6-SO3H.
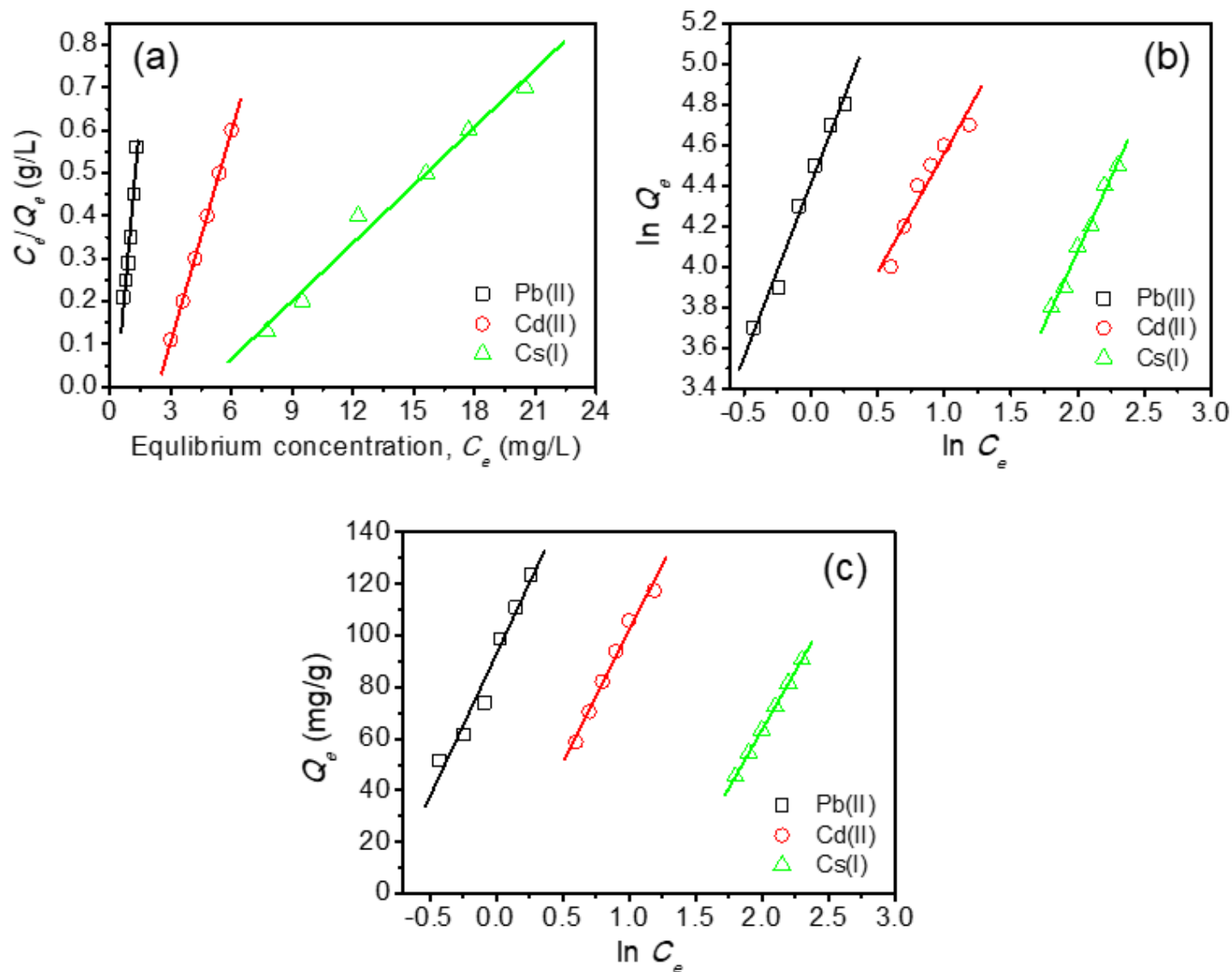
Figure 9

Fitting of adsorption isotherms of Pb(II), Cd(II) and Cs(I) ions into the functionalized mesoporous silica KIT-6-SO3H (a) Langmuir model, (b) Freundlich model and (c) Temkin model, respectively.

Supplementary Files

This is a list of supplementary files associated with this preprint. Click to download.

- Supportinginfo.docx
- graphicalabstract.docx